RESEARCH & DEVELOPMENT

UAV Selection Methodology and Performance Evaluation to Support UAV-Enabled Bridge Inspection

Ali Karimoddini, Ph.D.

Tara L. Cavalline, Ph.D., P.E.

Beth Smith, Ph.D., P.E.
Rodward Hewlin, Ph.D.
Abdollah Homaifar, Ph.D.

Autonomous Cooperative Control of Emergent Systems of Systems (ACCESS) Laboratory
Electrical and Computer Engineering Department
North Carolina A&T State University
1601 East Market Street
Greensboro, NC, 27411   **And**

The University of NC at Charlotte
9201 University City Blvd.
Charlotte, NC 28223-0001

1. Report No. FHWA/NC/2020-23	2. Government Accession No.	3. Recipient's Catalog No.
4. Title and Subtitle UAV Selection Methodology and Performance Evaluation to Support UAV-Enabled Bridge Inspection		5. Report Date March 15, 2022
		6. Performing Organization Code
7. Author(s) Ali Karimoddini, Tara L. Cavalline, Beth Smith, Rodward Hewlin, Abdullah Homaifar		8. Performing Organization Report No.

9. Performing Organization Name and Address
    North Carolina A&T State University, Electrical and Computer Engineering Department, 1601 East Market Street, Greensboro, NC, 27411, And
    University of North Carolina at Charlotte, Department of Engineering Technology and Construction Management, 9201 University City Blvd., Charlotte, NC 28223-0001
		10. Work Unit No. (TRAIS)

		11. Contract or Grant No.

12. Sponsoring Agency Name and Address North
    Carolina Department of Transportation
    Research and Development Unit
 	
    104 Fayetteville Street
    Raleigh, North Carolina 27601
		13. Type of Report and Period Covered
		    Final Report
		
		    August 1, 2019 – October 31, 2021

		14. Sponsoring Agency Code RP 2020-23
Supplementary Notes:		

16. Abstract

This project performed preliminary work to support use of Unmanned Aerial Vehicles (UAV)-based for bridge inspections, providing an economical and safer alternative to conventional inspection practices. The main challenge is that most existing technologies rely on general-purpose UAV platforms and there is no verified methodology for UAV-enabled bridge inspection principles and relevant considerations to reliably obtain inspection data. There have been some efforts to use general-purpose commercially available UAVs for bridge inspection. However, the turbulent environment that often exists around bridges requires customized and enhanced UAV platforms with a higher level of robustness, taking into account the bridge type and structure as well as the weather conditions around the bridge. Additionally, the data-acquisition capabilities of commercially available UAVs need to be compared to those required for bridge inspection. Previously, there has not been a study to quantify the gap between the performance of the commercially available UAVs and ideal desired performances. In this multidisciplinary project, a comprehensive set of experiments were developed for selection, testing, and evaluation techniques of candidate UAVs, the complex nature of flying UAVs in close proximity to bridges was explored, and the limitations of UAV flight due to turbulent flows around bridge components and nearby terrain was assessed. Commercially available platforms for bridge inspection were selected, tested, and evaluated. Deliverables from this project include: (1) measurable metrics to evaluate the performance of UAVs for bridge inspection, (2) experiments to test the suitability of UAVs for bridge inspection, and (3) a comprehensive analysis near-bridge environment flow field. Computational analysis of air flow patterns near bridge elements shows that the bridge geometry creates areas of turbulence and flow variation which impact the control requirements of the UAV. Local weather conditions can amplify these areas. Test flights were performed at selected structures to provide additional insight into the flight and data collection capabilities of the UAVs under consideration. Findings and deliverables from this project will help NCDOT justify capital purchases made to support UAV-assisted inspection, as well as additional research needed to integrate UAVs into their current bridge inspection processes. Ultimately, this work supports a follow-up project to develop workflows and implementation tools for efficient UAV-enabled bridge inspection.

17.		18. Distribution Statement	

19. Security Classif. (of this report)
    Unclassified
	20. Security Classif. (of this page)
	    Unclassified
		21. No. of Pages
		    65
			22. Price

Form DOT F 1700.7 (8-72)   **Reproduction of completed page authorized.**

DISCLAIMER

The contents of this report reflect the views of the author(s) and not necessarily the views of the University. The author(s) are responsible for the facts and the accuracy of the data presented herein. The contents do not necessarily reflect the official views or policies of either the North Carolina Department of Transportation or the Federal Highway Administration at the time of publication. This report does not constitute a standard, specification, or regulation.

ACKNOWLEDGMENTS

EXECUTIVE SUMMARY

The growing demand for the regular inspection of bridges requires more efficient and cost-effective alternative solutions. This project advanced the capabilities of NCDOT to use Unmanned Aerial Vehicles (UAV)-based bridge inspections to provide an economical and safer alternative to conventional inspection practices. The main challenge is that most existing technologies rely on general-purpose UAV platforms and there is no verified methodology for UAV-enabled bridge inspection principles and relevant considerations to reliably obtain inspection data. Hence, the goal of this multidisciplinary project was to address the complex nature of flying UAVs in close proximity of bridges by (1) providing a systematic procedure for selecting UAVs and (2) testing and evaluating the performance of commercially available platforms for bridge inspection in both computational fluid dynamic model simulations and field trials.

Deliverables from this project include: (1) measurable metrics to evaluate the performance of UAVs for bridge inspection, (2) experiments to test and evaluate the performance of the UAVs for bridge inspection, and (3) a comprehensive analysis of near-bridge environment flow fields.

Findings from this project revealed that there is great promise to use of UAVs to assist bridge inspectors working for NCDOT. The measurable metrics used to evaluate candidate UAVs for inspection identified during this work should allow NCDOT personnel to evaluate commercially available UAVs for purchase and use, as they aim to increase their inventory of UAVs to support this effort. The developed experiments can be used as a procedure for the certification of commercially available UAVs bridge applications. During this project UAVs from Digital Aerolus, Skydo, Intel, and Parrot participated in the experiments, and provided technical supports and insights during the experiments. As new technologies and other commercially available UAVs come to market, the capabilities and utility of other platforms can be assessed using the tests developed as part of this work. Our intention in this project was not to select a particular UAV, rather was to develop a procedure that can be used to select UAVs based on the priorities and desired parameters. Therefore, to avoid commercial advertisement and biasing toward any of the participant UAVs, we do not compare the performance of the UAVs with each other, and instead, we refer to the participant UAVs as UAV 1, UAV 2, UAV 3, and UAV4.

Computational fluid dynamics analysis of a selected bridge and the participant UAVs revealed that the commercially available UAVs should be capable of flying safely around most structural components. Solid elements such as the gusset plate in each diaphragm and the bents create regions of low velocity air. The UAV controls appear successfully transition from higher velocity regions through the open parts of the bridge geometry and the lower velocity, shielded regions. Maximum velocities and turbulence values near bridge elements are amplified by wind conditions. At this time specific weather guidelines have not been developed.

Flight tests performed at a ten-span structure using two UAVs provided insight into the feasibility and logistics associated with UAV-assisted inspection. Information regarding setup, workflow, and data collection was obtained, along with preliminary images that were compared to those presented in the most recent inspection report for the structure. The resolution of the images provided a level of detail comparable to that which was presented in the images included in the inspection report, providing confidence that the two candidate UAVs could be used to support UAV-assisted inspection.

Findings and deliverables from this project will help NCDOT justify capital purchases made to support UAV-assisted inspection, as well as additional research needed to integrate UAVs into their current bridge inspection processes. The findings from this project particularly enables a systematic approach for selection and certification of UAVs for bridge inspection. Findings from this project directly support a follow-up project, which will focus on developing workflows to support UAV-assisted bridge inspection and translation of UAV-obtained data into inspection reports. It is expected that adopting UAS-enabled bridge inspection will improve the quality of collected data through a stable flight system and enable conducting post-analysis of the acquired information for bridges' health diagnostics and assessment of their residual life.

TABLE OF CONTENTS

LIST OF TABLES

LIST OF FIGURES

1 INTRODUCTION AND RESEARCH OBJECTIVES

1.1 Introduction

There are about 13,500 bridges across the state of North Carolina (NC) highways. Impacts from traffic loads and natural deterioration and aging processes affect the condition of these bridges over the years. To ensure compliance with the National Bridge Inspection Standards (NBIS) requirements, and to facilitate planning of maintenance, repairs, rehabilitation, and replacement, the North Carolina Department of Transportation (NCDOT) regularly inspects all bridges at least every two years. Bridges differ in structure type based on (1) structural elements used, (2) what they carry, (3) materials used, (4) whether they are fixed or moveable, and (5) the terrain characteristics (e.g. what they span, onshore/nearshore). Like all states, North Carolina has a number of bridges that are classified as structurally deficient, and many bridges that are exhibiting distress due to natural aging and service conditions [1]. Although these bridges are safe to be used, inspections are required to ensure that their condition is known and the appropriate maintenance, repair, and rehabilitation activities are performed to allow these bridges to remain in service. The National Bridge Inspection Standards (NBIS) require all bridges require inspection every two years, with structurally deficient and other bridges of concern often requiring a more aggressive inspection plan. In addition to regular inspections, there are ad-hoc occasions that the bridges should be inspected for example after a flood or hurricane to ensure that they can be safely opened to the public.

The current inspection practices heavily rely on traditional approaches through which a team of specialized and certified inspectors conduct visual field inspections, sometimes in extremely difficult and risky conditions. It requires the inspectors to either climb and rappel or use mobile lift equipment (bucket lifts or "snooper trucks") or specific mobile assemblies to look for small defects and cracks in areas that are difficult to access or are at a high elevation from the ground below. Through this process detected deteriorations are manually documented, recorded, measured, and photographed. This manual process is often time consuming, and inaccuracies and variability can occur due to unavoidable human bias, experience, fatigue or errors. The information is recorded in the form of written reports and/or individual photos, which makes it difficult for agencies to employ advanced data-analytic techniques for post-processing and analysis of the detected problems. The American Society of Civil Engineers (ASCE) report, released in 2020, emphasizes the requirement of implementing more efficient and cost-effective alternative solutions for bridge inspection.

Considering the significant number of bridges across NC highways with a need for regular and ad-hoc inspections, particularly for those bridges that are structurally deficient, a more advanced bridge inspection approach is needed to facilitate the current manual inspection processes. Unmanned aerial vehicles (UAVs) provide a solution for this problem by carrying the sensing equipment around the bridges. However, commercially available UAVs cannot be directly used for bridge inspection, as the highly turbulent environment around the bridges could lead to the loss of control of drones under unfavorable conditions. Therefore, there is a need to develop test and evaluation techniques to assess the technological readiness level of commercially available UAVs for bridge inspection. In addition, there is a need for a better understanding of the near-bridge flow field which in turn impacts the robustness of the flight controllers to handle wind gust disturbances around the bridges.

1.2 Research Objectives

This multidisciplinary project develops test and evaluation techniques for candidate UAVs, explores and evaluates the complex nature of flying UAVs in close proximity to bridges, and assesses the limitations of UAV flight around bridges due to turbulent flows around bridge components and nearby terrain.

There have been some efforts to use general-purpose commercially available UAVs for bridge

inspection. However, the turbulent environment that often exists around bridges likely requires customized and enhanced UAV platforms with a higher level of robustness, taking into account the bridge type and structure as well as the weather conditions around the bridge. Additionally, the data-acquisition capabilities of commercially available UAVs need to be compared to those required for bridge inspection. Currently, there is no study to quantify the gap between the performance of the commercially available UAVs and ideal desired performances. To address this concern, there is a need to develop metrics to measure the performance of the UAVs for bridge inspection and design experiments to test and evaluate the UAVs by pushing them to the edge of their performance envelope. Further, near-bridge environments include irregular air motions characterized by winds that vary in speed and direction. These chaotic property changes, including low momentum diffusion, high momentum convection, and rapid variation of pressure and flow velocity in space and time determine the turbulence level of the area of interest. In addition to the chaos, diffusivity, flow rotation, three-dimensional asymmetric flow behavior, and dissipation are observed in a turbulent flow. Diffusivity enhances mixing and the increased rate of mass, momentum, and energy transport. The interaction among eddies of various scales passes energy sequentially from the larger eddies gradually to the smaller ones, known as turbulent energy cascade. The flow rotation and three-dimensional asymmetric flow behavior are associated with vortex stretching that define the turbulent energy cascade size. There have been relatively few studies on the near-bridge turbulence behavior. However, existing computational and experimental works show the importance of this phenomena in different areas, including drone-based bridge inspection, bridge design, and bridge aerodynamics.

To address these challenges and research needs, the goal of this project is to test and evaluate the performance of commercially available platforms for bridge inspection by achieving the following objectives:

- **Objective 1.1**: Develop metrics to measure the performance of the UAVs for bridge inspection.
- **Objective 1.2**: Design experiments to test and evaluate the performance of UAVs for bridge inspection.
- **Objective 1.3**: Test and evaluate the performance of some commercially available UAVs for the bridge inspection.

Remark: To avoid commercial advertisement and biasing toward any of the participant UAVs, we do not compare the performance of the UAVs with each other, and instead, we refer to the participant UAVs as UAV 1, UAV 2, UAV 3, and UAV4.

2   SUMMARY OF KEY LITERATURE FINDINGS

The 2021 bridge infrastructure data and reports show that there are 617,000 bridges in the United States, which play an important role in the transportation network. Among them, around 42% were built more than 50 years ago [1]. All bridges, particularly those that are aging, are subjected to natural deterioration. Therefore, in order to maintain the bridges' structural integrity and safety, regular inspection of bridges is required. Such practices obtain the required information about the health status of bridges for predictive and preventive maintenance. In total, as of 2019, around 231,000 bridges across the United States require repair and preservation work, even though they are still safe to be used. These bridges require more aggressive inspection plans and extensive maintenance schedules to remain in service.

Historically, bridge inspection has been performed by humans using a variety of access techniques, observation tools, and handheld equipment. Although human-based bridge inspection has served as the foundation of bridge management and safety assessment, conventional bridge inspection techniques are less efficient and can sometimes expose inspection personnel to danger and are subject to inefficiencies and error. To accomplish the required inspection tasks, inspectors rely on equipment including ropes, ladders,

lift trucks, and under-bridge inspection vehicles, which can be costly, often impact traffic flow, and may be viewed as risky to both inspectors and the travelling public from a safety perspective. Traffic control is often required, and travel lanes can be restricted during inspection activities, impacting the traveling public for significant durations. Additionally, the documentation and measurement process used by inspectors can be subject to human errors, bias, and limitations due to accessibility and visibility. Inspection personnel typically use textual descriptions and photos to document observed defects. The outcome of these recorded defects relies heavily on the experience of inspection personnel and can also be easily affected by the experience level or bias mood of the inspectors. In view of the challenges with the traditional inspection techniques, it is important to explore alternative inspection means or tools that can supplement the existing methods. UAVs and other types of mobile data acquisition systems have been identified seem to be a viable tool that can mitigate most of these challenges.

In [2], a mobile manipulator imaging system was employed for bridge inspection in which two CCD (charged-coupled device) cameras are installed to replace manual inspection. This solution addresses the safety and sensing-payload carrying issue, but it still suffers from traffic jams and logistic problems. These problems are addressed in [3] by making the carrier vehicle smaller and more agile, but it is limited to concrete bridges and still is too large to be used for train bridges [4]. The authors of [4] have improved the size of the vehicle; yet their design still has inherent mobility issues. An alternative solution to the above bridge inspection practices is to employ an Unmanned Aerial System (UAS) as a mobile sensing platform for bridge inspection. Employing UAS for inspection can significantly reduce the work accident risks, inspection cost and time, and required logistics, while enhancing the quality and reliability of the collected inspection data.

UAVs are of great interest to state highway agencies (SHA) to support a variety of activities, including surveying, emergency response, education and outreach, construction inspection, and condition inspection of a variety of infrastructure components [5, 6, 7, 8]. As UAV and supporting flight control and sensor technologies are rapidly improving, and are available at lower costs, many SHAs are establishing and supporting UAV programs to support a variety of objectives [9]. UAV-assisted bridge inspection is becoming increasingly enticing to many SHAs. All publicly owned in-service bridges must be inspected every two years, in accordance with the National Bridge Inspection Standards (NBIS) (23 CFR Subpart C). Inspection procedures are outlined in the AASHTO Manual for Bridge Evaluation (MBE) [10] and the Bridge Inspector's Reference Manual [11] and have historically relied upon visual and manual techniques performed by human inspectors.

Currently available UAV and sensor technologies have been found to be capable of supporting bridge inspection activities, providing improvements in access, reductions in traffic restrictions and cost, improvements in efficiency and safety, reduced environmental impacts, and enhanced data to support higher quality end inspection end products to support decision making [12]. UAVs have been targeted to support several types of bridge inspections, including initial/inventory, routine, in-depth, fracture-critical, special, and damage inspections. Specific inspection activities that can be supported by UAVs include [9]:

- Capturing images of areas and elements that are challenging or impossible for human access.

- Capturing data to support development of a 3-D model, supplementing 2-D photographs typically used to document structure conditions.

- Acquiring images and other data in a manner that can reduce human error and bias and can be used to monitor progression of deterioration over time.

The utility of a UAV for bridge inspection is a function of both its platform and its sensors. Most UAV currently used for bridge inspections are multirotor aircraft (not fixed wing aircraft) with a variety of sizes,

flight time capabilities, and sensor technologies. Operation of UAVs is governed by the requirements outlined in federal statutes 49 USC § 40102 and § 40105, and UAV operators are subject to FAA regulations. UAVs less than 55 pounds are subject to regulations outlined in 14 CFR Part 107, with additional requirements for UAVs greater than 55 pounds presented in 14 CFR Part 91. UAV operators must also comply with requirements associated with the airspace in which they plan to fly the UAV in Flying of UAV in the National Airspace System (NAS) requires compliance with a number of requirements, with FAA providing guidance at their website [9].

UAV can carry new miniaturized sensing technologies such as high-performance cameras, lidars, and thermal sensors which provide higher quality input to the state-of-the-art processing technologies such as Deep Learning [13, 14]. UAS has a significant potential in different transportation and civil engineering applications including but not limited to building inspection [15, 16, 17], transportation infrastructure assets [18, 19, 20], traffic surveillance [21, 22], safety inspection [23, 24], building facades inspection [24], surveying earthwork [26], and construction site monitoring [27, 28, 29]. Using UAS for bridge inspection is relatively new and sparse [30, 31, 32]. The application of UAS for inspection of Glued-Laminated Timber Arch Bridges is investigated in [33]. The ceiling effect for Contact-Based bridge inspection is studied in [34]. The employment of UAS for inspection of bridge beams is studied in [35]. A successful UAS-enabled bridge inspection procedure should address several challenges due to the UAS limitations (e.g., poor situational awareness due to poor visibility), bridge structure constraints (e.g., complex structure, turbulent flow fields around the bridge), environmental constraints (e.g., temperature, humidity), and site constraints (e.g., terrain characteristics). One of the recent efforts in the deployment of UAS for bridge inspection in the US is carried out by the Minnesota Department of Transportation [36]. While the project was not continued due to several flight crashes, one valuable outcome of the effort was highlighting the importance of understanding the required UAS specifications, considering the bridge and site limitations for a successful inspection. To the best knowledge of the authors, currently, there is not any verified comprehensive UAS-enabled solution for bridge inspection. Most existing case-dependent practices, including the work in [36], rely on general-purpose commercially available UAS platforms. There are currently a considerable number of general-purpose UAS commercially available, yet many new designs are continuously being introduced to this competitive market. The challenge is then to choose the best solution from the general-purpose UAS platforms for the specific application of bridge inspection.

This project explored UAVs feasibility for bridge inspection. UAVs are flown remotely either in autonomous mode or in manual mode by a pilot with the help of a controller. In the past, they were used by the military for combat and reconnaissance missions. However, in recent times, they have been used in applications such as, remote sensing [25], search and rescue missions [26], disaster management [27], courier services [28], security and surveillance [29], wireless coverage [30], precision agriculture [31], and infrastructure inspection [32]. The main drivers for the popularity are advances in UAV technologies and in remote sensing technologies such as light detection and ranging (LiDAR) and photogrammetry. In fact, bridge inspections seem to be the one application area that is receiving attention due to cost and safety advantages they offer. Use of UAV as a tool to supplement conventional bridge inspection methods will potentially provide a number of advantages. It can eliminate the risk associated with rope access and significantly lower the risk of access using other methods. In addition, it will provide cost savings, since use of specialized equipment such as snooper trucks, scaffolds, and man lifts can be reduced or eliminated. Use of UAVs will also provide time savings, reduce the amount of time bridge inspectors are at risk, and reduce traffic impacts. Furthermore, they offer real-time bridge inspection by means of mirroring the pilot screen onto another screen which can be viewed by inspectors. The inspectors can thus take a snapshot of identified defects for further examination later. Also, the remote sensing technologies for bridge inspections are non-contact techniques that lead to minimal traffic disruption. Finally, the collected data is a soft-copy and thus it makes the easy application of advanced data analysis techniques.

The main challenge that restricts the use of UAVs for bridge inspection is government regulations. For

example, Federal Aviation Authority (FAA) regulations forbid UAV flying on traffic or persons not directly involved in the inspection. Also, there is also the restriction of beyond-line-of-sight flight [17]. The UAV capability to operate in a GPS-denied environment [37], bad weather [33] and its flight duration also limits viability for bridge inspection. The small size of the UAV makes them susceptible to wind gusts rendering them difficult to control during inspection [33]. In addition, some bridge inspection tasks requiring physical contact, such as determining the width of cracks, cleaning bridge elements to remove rust or dust for detailed defect observation cannot be accomplished with UAVs [33]. Finally, there is no available comprehensive guide on testing the various UAV criteria for a specific task. This is particularly important for inspectors to have a fair idea of how the chosen UAVs will perform when used for inspection.

There are some existing studies that have explored the viability of UAVs for bridge inspection. For instance, [17] investigated UAV-enabled bridge inspection methodology which led to the development of a five-stage bridge inspection workflow: bridge information review, site risk assessment, pre-flight setup, UAVs-enabled inspection and data processing. The main criteria for UAV selection were based on flight time, upward viewing camera capability, camera resolution, video resolution, payload capacity, illumination and communication range. Minnesota DoT in collaboration with Collins Engineering reported their findings on the challenges and benefits of UAVs for bridge inspection [34]. This work was carried out using four different bridges in order to evaluate the effectiveness of the UAVs for inspecting different types of bridges. The Michigan Department of Transportation also explored UAV-enabled bridge inspection using 5 different UAVs for bridge inspection [35]. This work also highlighted the effectiveness of a particular UAV as a supplementary tool for bridge inspection.

The previous studies that explored UAVs for bridge inspection placed less emphasis on the UAV selection. In most cases no test was conducted by the authors to verify if the UAV can withstand bridge conditions. As a result of the sole reliance on information in the specification documents, important criteria such as RF immunity and GPS robustness is rarely taken into consideration during UAV selection. Therefore, in this work, a comprehensive list of important UAV criteria for bridge inspection is presented. In addition, experiments are developed to test these features.

3 IDENTIFYING CANDIDATE COMMERCIALLY AVAILABLE UAVS FOR THE BRIDGE INSPECTION

3.1 Introduction

Considering the enormous number of bridges in the United States, inspection process improvements have a significant impact on public safety, transportation system effectiveness (i.e., availability), and maintenance/repair/rehabilitation/replacement procedures (i.e., scheduling, cost, and impact to the traveling public) of bridges. As our nation's highway infrastructure system ages and expands to accommodate a growing population, the resources required to build, maintain, and inspect our bridge inventory will increase. Despite the growing demand for the regular inspection of bridges, the current practices heavily rely on traditional approaches through which a team of specialized and certified inspectors conducts visual field inspections, sometimes in extremely difficult and risky conditions. This manual process is time-consuming and inaccurate due to unavoidable human errors (e.g., the level of workers fatigue and experience). Further, this manual procedure reduces the possibility of accurate multimodal sensing documentation for offline post-inspection processes due to the limited amount of equipment an inspector can carry. These manual and labor-intensive inspection procedures often lead to traffic-flow (e.g., when an inspection vehicle blocks lanes, or lanes are closed to traffic to protect inspectors on foot) interruptions and introduces unnecessary safety risks to both inspector and the public. Therefore, innovative bridge inspection practices, as an enabling step of any maintenance planning, have been of interest to researchers to evaluate the feasibility of deploying emerging technologies [38].

This report addresses the existing research gap of selecting a suitable UAS platform for a bridge inspection mission. A systematic framework for ranking available UAS candidates is developed based on three key factors: (1) UAS capabilities and limitations, (2) UAS sensing capabilities, and (3) UAS reaction to environmental parameters. An Analytical Hierarchy Process (AHP) methodology is adopted for the multiple-criteria decision-making (MCDM) process. In this hierarchical method, four major categories including Flight Performance, Situational Awareness, Payload and Sensor Capabilities, and Communication Quality are defined. Within Each category, multiple criteria are defined and compared pairwise. This AHP method results in a sorted list of criteria which are more important for selection of UASs for bridge inspection. Then, the outcome of AHP is applied to a set of commercial UASs, and the comparison result is provided for three UASs.

Table 3.1: Defined criteria for selection of UAS-enabled bridge inspection.

Parameter	Explanation
Flight Performance	
Endurance	Maximum flight time with one fully charged battery (minutes)
Wind Tolerance	Maximum wind speed in which the UAS can operate safely (meters/seconds)
Gusts Tolerance	Maximum wind gust in which the UAS can operate safely (meters/seconds)
Max Altitude	The highest altitude UAS can reach (meters MSL)
Net Weight	The weight of the functional UAS excluding its sensors (kilograms)
Environmental Temperature Range	The temperature range of the environment in which the UAS can safely operate (Centigrade)
Autonomy	The capability of operating autonomously with minimum human interactions
Number of Engines	The number of engines UAS is equipped with
Max Climb Rate	Maximum vertical speed UAS can achieve (meters/seconds)
Max Airspeed	Maximum horizontal speed UAS can achieve with respect to the air (meters/seconds)
All-weather ability	The capability of operating in different weather conditions
Physical Protection	The cage, ring, shroud, or similar measures installed to reduce the risk of damage caused by propellers in case of a crash
Situational Awareness	
NavCam	The capability of perceiving the surrounding area visually through Navigational Cameras

GNSS	The accuracy of on-board equipment to utilize Global Navigation Satellite Systems
Ultrasonic	The capability of perceiving the surrounding area and measuring distance to obstacles using ultrasonic sensors
Gyro	The accuracy and update rate of the installed gyro
Accelerometer	The accuracy and update rate of the installed accelerometer
Compass	The accuracy and update rate of the installed compass
Magnetometer	The accuracy and update rate of the installed magnetometer
Barometer	The accuracy and update rate of the installed narometer
Beyond Line-Of-Sight Range	The radius in which UAS can safely operate without being in the line of sight of pilot or human supervisor (meters)
RTK	The accuracy and update rate of the installed Real Time Kinematics
Payload and Sensor Capabilities	
Can look upward?	Capability of mounting sensor to look upward
Can carry custom payload?	Capability of carrying custom payloads
Max payload weight	Maximum weight UAS can carry (kilograms)
Default payload	The default sensor
Communication Quality	
Frequencies	Frequencies UAS is using for both RC and streaming data
Low Latency	The delay of streamed data
Live Stream	Capability of streaming sensor data online
Communication Range	The maximum distance UAS can send data (meters)
RC Range	The maximum distance UAS can be controlled using Remote Controller (meters)
Encryption	Capability of Encrypting Communication channels

3.2 Background

Multiple-criteria decision-making (MCDM), also known as Multi-Criteria Decision Analysis (MCDA), is an approach towards the decisions involving the choice of the best alternative among several potential candidates by explicitly evaluating multiple conflicting criteria [39]. In MCDM, which is a field of

operational research, potential candidates are assessed to select the most suitable alternative which satisfies the desired goal with respect to the set of multiple and often conflicting criteria, e.g., customer satisfaction and the cost of providing service in the service industry [37, 40].

Different scenarios have different degrees of risk, fuzziness, and uncertainty; therefore, different methods of MCDA are developed to be compatible with different scenarios. The Simple Multi-Attribute Rating Technique (SMART) [41], SWING weighting [42], TRADEOFF weighting [43], and Analytical Hierarchy Process (AHP) [44] are some of the more well-known MCDA methods in the literature. Among these methods, AHP has been a popular method for MCDM applications including but not limited to sustainable energy planning [45], wind farm site selection [46], bidding decision making [47], maintenance planning of reinforced concrete [48], post-disaster sustainability analysis [49], classification of areas suitable for fish farming [50], and safety evaluation of urban public parks [51].

AHP employs a hierarchical weighting mechanism, where each layer conducts a comparison between each pair of nodes [44]. From the top to the bottom layers of an AHP hierarchical structure, the layers include nodes of goal, categories, criteria, or candidates/alternatives. The weighting mechanism within the AHP technique is conducted based on the values provided in Table 3.2 to assist judgements (pairwise comparisons between nodes). These judgments are conducted to convert quality to quantity and establish a partial order relation based on the pairwise comparison over a set of nodes. After establishing these pairwise relations, the relative weight of each component in the table can be found. The inconsistency of judgments (violation of transitivity or anti-symmetric relations) can be numerically captured via the consistency ratio, CR, which is calculated over the reciprocal matrices containing the results of the judgments. The consistency ratio CR is related to the largest eigenvalue λ_{max} in the reciprocal matrix. To mathematically define CR, [44] introduced the consistency index CI as $CI = \frac{\lambda_{max} - n}{n-1}$ where n is the number of nodes we are comparing (the number of rows/columns of the reciprocal matrix). Then, the consistency ratio CR can be defined as:

$$CR = \frac{CI}{RI}$$

Where RI is the random consistency index that provides the average CI of randomly generated comparisons [44]. The comparison matrix might be reconstructed if the CR value exceeds a certain threshold, e.g., 10%.

Table 3.2: The scaling mechanism of pairwise comparisons within the AHP methodology

Intensity of Importance	Definition	Explanation
1	Equal importance	Two activities contribute equally to the objective
3	Moderate importance of one over another	Experience and judgment slightly favor one activity over another
5	Essential or strong importance	Experience and judgment strongly favor one activity over another
7	Extreme importance	An activity is favored very strongly, and its dominance is demonstrated in practice

9	Extreme importance	The evidence favoring one activity over an-other is of the highest possible order of affirmation
2,4,6,8	Intermediate values	When compromise is needed

3.3 Methodology

The goal of the deployed AHP in this research study was to select suitable UAS characteristics that can best conduct bridge inspection. In the hierarchical structure of the deployed AHP, four categories were used. Within each category, multiple criteria were identified. The list of all categories and their associated criteria are listed in Table 3.1. This section will provide a description and pairwise comparison of the categories and their associated criteria. Then, the candidate UASs are compared against each other with respect to each criterion. A detailed description of the categories, criteria, candidate UASs, and their pairwise comparison matrices are provided in the next subsections.

3.3.1   Comparison and Description of Categories

In the hierarchical structure of the deployed AHP, four categories were used, including Flight Performance, Situational Awareness, Payload and Sensor Capabilities, and Communication Quality:

- *Flight Performance* category refers to flight characteristics of UASs in terms of physical properties, flight dynamical properties, and autonomy capabilities of UASs
- *Situational Awareness* category concerns about how well a UAS can perceive the surrounding environment.
- *Payload and Sensor Capabilities* category reflects the sensing features and the potential for carrying the required sensors; and
- *Communication Quality* category represents the factors contributing to the quality of communication links.

The list of all categories and their associated criteria are listed in Table 3.1. The pairwise comparison of these categories is provided in Table 3.3. For example, Flight Performance is extremely more important to consider for the selection of a UAS than Communication Quality, as most UASs are equipped with relatively reliable long-range communication devices which is sufficient for bridge inspection, where the pilot/ground station is relatively close to the inspection site. Therefore, using the guideline provided in Table 3.2. Other elements of the table are filled with similar reasoning, based on experts' opinion and the available literature. Note that Table 3.3 only shows the upper triangular components, understanding that the lower part can be obtained as the inverse of the components that are symmetric with respect to the matrix diagonal.

3.3.2   Comparison and Description of Criteria

3.3.2.1 Flight Performance

This category contains parameters such as the flight performance of UASs including flight and dynamical characteristics of UASs, autonomous flight performance capabilities, and physical properties of UASs that are important for the selection of UASs for the bridge inspection purpose. The list of criteria under this category and their description is provided in Table 3.4. The pair-wise comparison for the criteria under Flight Performance category is provided in Table 3.5. For example, Gusts Tolerance is a very important factor for a bridge inspection mission because even smallest amounts of wind can interact with the structure of the bridge, resulting in areas with turbulent air mass powerful enough to impact the physical behavior of

UAS flying close to the bridge [52, 53, 54]. Therefore, Gusts Tolerance has a relatively higher value (intensity of importance) compared to other criteria.

3.3.2.2 Situational Awareness

For bridge inspection, good autonomy results in more stable flights. It provides the opportunity for collecting higher quality and more consistent data. However, higher levels of autonomy require more advanced situational awareness systems. On the other hand, in aviation, safety is a crucial factor [55] which cannot be achieved without accurate and comprehensive situational awareness [56]. In general, manned aviation, situational awareness includes details of the aircraft's operational parameters, external conditions, navigational information, the status of the aircraft, and hostile factors [57]. Higher, or at least the same, expectations are required for an (autonomous or piloted) unmanned aircraft. This is due to the fact that despite all arrangements to meet the general requirement of maintaining constant line of sight, enforced by Federal Aviation Administration (FAA) [58], due to the structure of the bridge, the line of sight might be interrupted, where a proper situational awareness is critical in such a challenging environment. Situational awareness is generally obtained by processing the data gathered from (onboard) sensors. These sensors can be different from the main sensors which are supposed to acquire data for the bridge inspection mission, and include Navigational Cameras (NavCam), Global Navigation Satellite System (GNSS); Real-time kinematic (RTK) positioning, gyro, accelerometer, compass, magnetometer, barometer for accurate determining the position, orientation, and acceleration of the UAS, as well as the range that the UAS may travel autonomously beyond the line of sight. The comparison of these criteria for assessment of situational awareness is given in Table 3.6. and 3.7.

3.3.2.3 Payload and Sensor Capabilities

The goal of a bridge inspection mission is to gather data employing specific sensors. Some aircraft are equipped with a sensor that cannot be changed while others are capable of carrying custom sensor payloads. While the default sensor of the aircraft is important, the maximum weight of the custom payload is also a decision parameter for selecting an aircraft for bridge inspection. One of the main advantages of using UAS for bridge inspection is the possibility to easily gather data from surfaces that are difficult to access with other approaches. Such surfaces might be located beneath certain bridge elements (such as the underside of a bridge deck), or in hard to access areas (such as the bearings of girders). Therefore, in addition to being able to collect data in lateral and downward directions (which is a common capability of almost all general-purpose UASs), it is important that the UAS be able to look upward and rotate to gather data for bridge inspection. These considerations about payload and sensor capabilities are included under Payload and Sensor Capabilities category and are compared in Table 3.7.

3.3.2.4 Communication Quality

A UAS may communicate with the Ground Control Station for two purposes: (1) to receive control and command signals via the radio link, and (2) to transmit sensor readings. The communication must be done via reliable frequency channels. For the radio link, the ground human operators need to use long-range remote controllers (RC). Further, it is important to send encrypted and low-latency control and command signals to the UAS. On the other hand, for the data link, it is important to live-stream large volumes of data (e.g., video feed) as the on-board storage usually is not sufficient to save the entire mission data. These concerns are included in the Communication Quality category and have been compared under Table 3.8.

Table 3.3: AHP comparisons for categories.

	Flight	Situational	Payload & Sensor	Communication	Weight

	Performance	Awareness	Capabilities	Quality	
Flight Performance	1	2	1	9	0.389
Situational Awareness		1	1	9	0.281
Payload & Sensor Capabilities			1	5	0.287
Communication Quality				1	0.043

Table 3.4: The technical details and Criteria values for candidate UAS platforms.

Parameter	UAV 2	UAV 1	UAV 3	UAV 4
Flight Performance				
Endurance (mins)	25	23	16-26	5
Wind Tolerance (m/s)	13.5	11	12-16	5
Max Altitude (m MSL)	4500	4572	4000	N/A
Net Weight (kg)	0.32	0.775	1.2	2.69
Environmental Temperature Range (centigrade)	-10 to 40	-5 to 40	-5 to 40	-20-40
Autonomy	Yes	Yes	Yes	No
Number of Engines				
Max Climb Rate (m/s)	4	4	10	5
Max Airspeed (m/s)	15.3	16	10	Pilot dependent
All-weather ability	No	No	No	No
Physical Protection	No	No	Yes	No
Situational Awareness				

NavCam	N/A	360	N/A	1 FPV
GNSS	GPS& GLONASS	AGPS	GPS, GLONASS	GPS
Ultrasonic	N/A	N/A	N/A	N/A
Gyro	N/A	31 milli rad/s @ 8KHz	N/A	N/A
Accelerometer	N/A	88_g@4kHz	N/A	N/A
Compass	N/A	N/A	N/A	N/A
Magnetometer	N/A	N/A	N/A	N/A
Barometer	N/A	+/- 0.1 hPa; 25Hz	N/A	N/A
Beyond Line-Of-Sight Range	Battery or mission dependent	3500	Yes	N/A
RTK	N/A	N/A	N/A	N/A
Payload and Sensor Capabilities				
Can look upward?	Yes	Yes	Yes	Yes
Can carry custom payload?	Yes	No	No	No
Max payload weight (kg)	N/A	0.1	0.8	0.5
Default payload	4k Camera/Thermal	3axis gimbal, Color Camera - 1/2.3" 12.3MP CMOS	Sony Alpha 7R	Sony EOXII and FLIR Boson 320
Communication Quality				
Frequencies	Wi-Fi 802.11a/b/g/n 2.4 - 5.8 GHz	2.4-2.483; 5.18-5.24; 5.725-5.85 GHz	2.4GH (2x Diversity control/data links), 5.8 GHz	2.4 GHz, 5.8 GHz
Low Latency	Yes	Yes	Yes	Yes
Live Stream	Yes	No	Yes	Yes
Communication Range (m)	4000	3500	1000	6920

RC Range (meters)	4000	3500	1000	6920
Encryption	WPA2	Yes	Yes	Yes

Table 3.5: AHP comparisons for Flight Performance criteria

	Endurance	Wind Tolerance	Gusts Tolerance	Max Altitude	Net Weight	Env. Temp.	Autonomy	Number of Engines	Max Climb Rate	Max Airspeed	All-weather ability	Physical Protection	Weights
Endurance	1	1/3	1/5	5	3	3	1/3	5	5	5	1	3	0.098
Wind Tolerance		1	1/3	3	3	3	1/3	1	7	3	1	2	0.102
Gusts Tolerance			1	9	5	5	3	5	9	9	5	1	0.238
Max Altitude				1	1/5	1/5	1/9	1/5	1	1	1/7	1/5	0.016
Net Weight					1	3	1/5	1	3	3	1/3	1/5	0.051
Env. Temp.						1	1/9	1	3	3	1/3	1/5	0.038
Autonomy							1	7	7	7	3	5	0.206
Number of Engines								1	3	3	1	1	0.048
Max Climb Rate									1	1	1/5	1/5	0.017
Max Airspeed										1	1/5	1/3	0.019
All-weather ability											1	1/2	0.080
Physical Protection												1	0.086

Table 3.6: AHP comparisons for the Situational Awareness criteria

	NavCam	GNSS	Ultrasonic	Gyro	Accelerometer	Compass	Magnetometer	Barometer	Beyond Line-Of-Sight Range	RTK	Weights
NavCam	1	3	1/3	1/5	1/3	1	3	3	5	1/3	0.073
GNSS		1	1/3	1/5	1/3	1	3	5	3	1/3	0.060
Ultrasonic			1	1/3	5	3	5	5	7	1/3	0.172
Gyro				1	1	3	7	5	7	1	0.208
Accelerometer					1	5	7	7	5	1	0.166
Compass						1	1	3	3	1/3	0.054
Magnetometer							1	3	3	1/5	0.038
Barometer								1	1	1/5	0.023
Beyond Line-Of-Sight Range									1	1/9	0.020
RTK										1	0.185

Table 3.7: AHP comparisons for Payload and Sensor criteria

	Can look upward?	Can carry custom payload?	Max payload weight	Default payload	Weights
Can look upward?	1	7	9	7	0.702
Can carry custom payload?		1	1	1	0.095
Max payload weight			1	1/3	0.072
Default payload				1	0.131

Table 3.8: AHP comparisons for Communication Quality criteria

	Frequencies	Low Latency	Live Stream	Communication Range	RC Range	Encryption	Weights
Frequencies	1	1	1	1/3	1/3	5	0.112
Low Latency		1	1/3	1/5	1/5	3	0.074
Live Stream			1	1/3	1/3	5	0.134
Communication Range				1	1	9	0.326
RC Range					1	9	0.326
Encryption						1	0.029

3.3.2.5 Results

Table 3.3 provides the pairwise comparison of the categories as explained in Section 2. The relative weights are provided in the weight column of Table 3.3. A similar procedure is applied to find the relative weights of criteria in Flight Performance, Situational Awareness, Payload and Sensor Capabilities, and Communication Quality categories, shown in the weight column of Tables 3.5, 3.6, 3.7, and 3.8, respectively. From the relative weight of the criterion in each category, the overall relative weight of each criterion, the Total Weight column in Table 3.9, can be calculated by multiplying the criterion weight by the weight of the category to which the criterion belongs to, i.e., Category Weighting-category Weight columns. Table 3.9 contains the criteria sorted by their relative total weights. As can be seen from Table 3.3, the Flight Performance category has the highest weight, followed by Payload and Sensor Capabilities, Situational Awareness, and Communication Quality. The overall results in the compiled Table 3.9 follows a similar pattern, where the top half of the table is mainly dominated with criteria within the Flight Performance category. Yet, some criteria have been elevated or demoted by the hierarchical mechanism of the AHP. For instance, the importance of the capability of looking upward and collecting data from surfaces which are placed beneath the bridge has elevated the weight of the Can look upward? criterion and placed it at the top of the table. On the other hand, the candidates are compared and their relative weights with respect to each criterion are shown Underweight columns of Table 3.10

Table 3.9: Criteria sorted by their relative total weights

Criterion	Category Weight	In-category Weight	Total Weigh	Category
Can look upward?	0.287	0.702	0.2015	Payload and Sensor
Gusts Tolerance	0.389	0.238	0.0926	Flight Performance
Autonomy	0.389	0.206	0.0801	Flight Performance
Gyro	0.281	0.208	0.0584	Situational Awareness
RTK	0.281	0.185	0.0520	Situational Awareness

Ultrasonic	0.281	0.172	0.0483	Situational Awareness
Accelerometer	0.281	0.166	0.0466	Situational Awareness
Wind Tolerance	0.389	0.102	0.0397	Flight Performance
Endurance	0.389	0.098	0.0381	Flight Performance
Default Payload	0.287	0.131	0.0376	Payload and Sensor
Physical Protection	0.389	0.086	0.0335	Flight Performance
All-weather ability	0.389	0.080	0.0311	Flight Performance
Custom payload?	0.287	0.095	0.0273	Payload and Sensor
Max Payload weight	0.287	0.072	0.0207	Payload and Sensor
NavCam	0.281	0.073	0.0205	Situational Awareness
Net Weight	0.389	0.051	0.0198	Flight Performance
Number of Engines	0.389	0.048	0.0187	Flight Performance
GNSS	0.281	0.060	0.0169	Situational Awareness
Compass	0.281	0.054	0.0152	Situational Awareness
Environmental Temperature Range	0.389	0.038	0.0148	Flight Performance
Communication Link Range	0.043	0.326	0.0140	Communication Quality
RC Range	0.043	0.326	0.0140	Communication Quality
Magnetometer	0.281	0.038	0.0107	Situational Awareness
Max Airspeed	0.389	0.019	0.0074	Flight Performance
Max Climb Rate	0.389	0.017	0.0066	Flight Performance
Barometer	0.281	0.023	0.0065	Situational Awareness
Max Alt.	0.389	0.016	0.0062	Flight Performance
Live stream	0.043	0.134	0.0058	Communication Quality
Beyond-Line-Of-Sight Range	0.281	0.020	0.0056	Situational Awareness
Frequencies	0.043	0.112	0.0048	Communication Quality

Low latency	0.043	0.074	0.0032	Communication Quality
Encryption	0.043	0.029	0.0012	Communication Quality

Verified by the consistency ratio, the results under the category, criteria, and candidate tables are consistent. The CR values for Category table, Table 3.3, is 4.8%, and for the criteria within Flight Performance, Situational Awareness, Payload and Sensor Capabilities, and communication Quality are 9.4%, 9.9%, 5.8%, and 2.5%, respectively; all of them are less than 10% as the defined threshold. Further, the sub-tables for candidates' comparison in Table 3.10 are all less than 10% as well.

With these consistent tables, the final score of each candidate UAS can be calculated, which shows the numerical representation of candidate's suitability with respect to the bridge inspection. the final score of each candidate UAS is calculated as:

$$S = \sum_i s_i w_i$$

where is the candidate's score for the ith criterion, extracted from the Score columns of Table 3.10, and w_i is the total weight of that criterion, extracted from the Total Weight in Table 3.9. The criterion score of each candidate and its final score are presented in Table 3.11 As it is shown in the last row of Table 3.11, the final score of candidates A, B, C and D are 0.2549, 0.2577, 0.2743, and 0.2345, respectively; the candidate C is the most suitable choice.

Table 3.10: AHP comparisons for candidate comparison with respect to each criterion.

	UAV 2	UAV 3	UAV 1	UAV 4	Weights	UAV 2	UAV 3	UAV 1	UAV 4	Weights	UAV 2	UAV 3	UAV 1	UAV 4	Weights	UAV 2	UAV 3	UAV 1	UAV 4	Weights
Criteria	Can look upward?					Gusts Tolerance					Autonomy					Gyro				
UAV 2	1	1	1	1	0.25	1	1/3	1	5	0.29	1	1	1	5	0.31	1	1	1	1	0.25
UAV 3		1	1	1	0.25		1	3	6	0.35		1	1	5	0.31		1	1	1	0.25
UAV 1			1	1	0.25			1	5	0.29			1	5	0.31			1	1	0.25
UAV 4				1	0.25				1	0.29				1	0.06				1	0.25
Criteria	RTK					Ultrasonic					Accelerometer					Wind Tolerance				
UAV 2	1	1	1	1	0.25	1	1	1/5	1	0.13	1	1	1	1	0.25	1	1/4	1	3	0.27
UAV 3		1	1	1	0.25		1	1/5	1	0.13		1	1	1	0.25		1	1/4	4	0.36
UAV 1			1	1	0.25			1	5	0.63			1	1	0.25			1	3	0.27
UAV 4				1	0.25				1	0.13				1	0.25				1	0.09
Criteria	Endurance					Default Payload					Physical Protection					All-weather ability				
UAV 2	1	3	1	5	0.5	1	5	4	3	0.23	1	1	1	1/5	0.13	1	1	1	1	0.25
UAV 3		1	1/3	1	0.1		1	1/3	5	0.39		1	1	1/5	0.13		1	1	1	0.25
UAV 1			1	3	0.3			1	5	0.31			1	1/5	0.13			1	1	0.25
UAV 4				1	0.1				1	0.08				1	0.625				1	0.25
Criteria	Custom payload?					Max Payload weight					NavCam					Net Weight				
UAV 2	1	1	1	1	0.25	1	1	1	1	0.25	1	1	1	1	0.25	1	1	1	1	0.25
UAV 3		1	1	1	0.25		1	1	1	0.25		1	1	1	0.25		1	1	1	0.25
UAV 1			1	1	0.25			1	1	0.25			1	1	0.25			1	1	0.25
UAV 4				1	0.25				1	0.25				1	0.25				1	0.25
Criteria	Number of Engines					GNSS					Compass					Env. Temp.				
UAV 2	1	1/5	1	1	0.13	1	1	1	1	0.25	1	1	1	1	0.25	1	2	2	1/4	0.13
UAV 3		1	1/5	5	0.63		1	1	1	0.25		1	1	1	0.25		1	1	1/2	0.25
UAV 1			1	1	0.13			1	1	0.25			1	1	0.25			1	1/4	0.13
UAV 4				1	0.13				1	0.25				1	0.25				1	0.50
Criteria	Comm. Range					RC Range					Magnetometer					Max Airspeed				
UAV 2	1	1	1	1/2	0.2	1	1	1	1/2	0.2	1	1	1	1	0.25	1	1	1	1	0.25
UAV 3		1	1	1/2	0.2		1	1	1/2	0.2		1	1	1	0.25		1	1	1	0.25
UAV 1			1	1/2	0.2			1	1/2	0.2			1	1	0.25			1	1	0.25
UAV 4				1	0.4				1	0.4				1	0.25				1	0.25
Criteria	Max Climb Rate					Barometer					Max Altitude					Live stream				
UAV 2	1	1/2	1	1	0.2	1	1	1	1	0.25	1	1	1	1	0.25	1	1	1	1	0.25
UAV 3		1	1	2	0.4		1	1	1	0.25		1	1	1	0.25		1	1	1	0.25
UAV 1			1	1	0.2			1	1	0.25			1	1	0.25			1	1	0.25
UAV 4				1	0.2				1	0.25				1	0.25				1	0.25
Criteria	Beyond LOS Range					Frequencies					Low latency					Encryption				
UAV 2	1	1	1	1	0.25	1	1	1	1	0.25	1	1	1	1	0.25	1	1	1	1	0.25
UAV 3		1	1	1	0.25		1	1	1	0.25		1	1	1	0.25		1	1	1	0.25
UAV 1			1	1	0.25			1	1	0.25			1	1	0.25			1	1	0.25
UAV 4				1	0.25				1	0.25				1	0.25				1	0.25

Table 3.11: The criterion scores of candidates UASs and their final score

	UAV 2	UAV 3	UAV 1	UAV 4	Criterion Weight
Can look upward	0.0504	0.0504	0.0504	0.0504	0.2015
Gusts Tolerance	0.0272	0.0327	0.0272	0.0272	0.0926
Autonomous	0.0251	0.0251	0.0251	0.0050	0.0801
Gyro	0.0146	0.0146	0.0146	0.0146	0.0584
Ultrasonic	0.0060	0.0060	0.0302	0.0060	0.0483
Accelerometer	0.0117	0.0117	0.0117	0.0117	0.0466

Wind Tolerance	0.0108	0.0145	0.0108	0.0036	0.0397
Endurance	0.0191	0.0038	0.0114	0.0038	0.0381
Defualt Payload	0.0087	0.0145	0.0116	0.0029	0.0376
All-weather ability	0.0078	0.0078	0.0078	0.0078	0.0311
Custom payload?	0.0068	0.0068	0.0068	0.0068	0.0273
Max Payload weight	0.0052	0.0052	0.0052	0.0052	0.0207
NavCam	0.0051	0.0051	0.0051	0.0051	0.0205
Net Weight	0.0050	0.0050	0.0050	0.0050	0.0198
Number of Engines	0.0047	0.0047	0.0047	0.0047	0.0187
GNSS	0.0042	0.0042	0.0042	0.0042	0.0169
Compass	0.0038	0.0038	0.0038	0.0038	0.0152
Environmental Temperature Range	0.0019	0.0037	0.0019	0.0074	0.0148
Communication Link Range	0.0028	0.0028	0.0028	0.0028	0.0140
RC Range	0.0028	0.0028	0.0028	0.0028	0.0140
Magnetometer	0.0027	0.0027	0.0027	0.0027	0.0107
Max Airspeed	0.0019	0.0019	0.0019	0.0019	0.0074
Max Climb Rate	0.0013	0.0026	0.0013	0.0013	0.0066
Max Alt.	0.0016	0.0016	0.0016	0.0016	0.0062
Live stream	0.0015	0.0015	0.0015	0.0015	0.0058
Beyond Line-Of-Sight Range	0.0014	0.0014	0.0014	0.0014	0.0056
Frequencies	0.0012	0.0012	0.0012	0.0012	0.0048
Low latency	0.0008	0.0008	0.0008	0.0008	0.0032
Encryption0.0003	0.0003	0.0003	0.0003	0.0003	0.0012
Final Score	0.2549	0.2577	0.2743	0.2345	1

Important note: *The comparisons, numbers, and results presented in this paper, similar to any other MCDA, are highly case-dependent. Although the initiated framework development can be applied to other case studies, the presented results in this paper reflect the surveyed expert and the authors' opinions. Therefore, as long as the pair-wise comparisons meet the AHP's consistency constraint, the developed systematic framework in this paper can be adjusted to take into account the preferences of a new case study.*

4 DEVELOPMENT OF COMPUTATIONAL FLUID DYNAMICS (CFD) MODELS OF UAVS FLYING NEAR, ALONGSIDE, AND WITHIN A BRIDGE

4.1 Background

A number of US states have performed research supporting deployment of UAVs to assist with bridge inspections [36, 59, 60, 61, 62, 63]. Many of these studies have focused on establishing and enhancing the capabilities of the UAVs to obtain the desired/required inspection data and support development of end products such as inspection reports. However, other challenges exist that must be addressed before UAVs can be moved from experimental technologies to standard use. Bridges are typically unique structures, varying in construction details and terrain configuration, and exposed to a variety of weather conditions. Issues such as wind gusts and wind-structure interaction can impact stand-off distances and the capability of a UAV to gather the data needed. Weather conditions and tight structural constraints can provide challenging conditions for flight, and UAVs can be damaged or lost during inspection activities. A better understanding of the fluid dynamics in the near-structure environment will help to optimize the flight and data acquisition parameters required for successful use of UAVs to support bridge inspection. These parameters include flight mode, standoff distance, flying speed, camera pointing angles, camera parameters, and flight planning for weather conditions and future post-processing [64]. As a result, the goal of the present work is to analyze the aerodynamic performance of a Skydio 2 UAV as a supplementary tool for bridge girder inspections. The numerical prediction methodology, problem setup, as well as assessment of parametric results are discussed in further detail.

4.2 Collection of Weather Data

To support development of computational fluid dynamics (CFD) models of UAVs flying near, alongside, and within bridge structures, weather data was collected at a bridge on US 70 Eastbound (structure 4) over the East End Connector in Durham, NC. The weather station was mounted in three positions, capturing data above the deck, alongside the bridge, and at an interior position within the girders of the bridge (on a diaphragm). Weather data collected included temperature, humidity, wind speed, gust speed, and wind direction. In total, weather data was collected for approximately 4 months to support CFD modeling, with at least one month worth of data collected at each mounting position.

Figure 4.2: Location weather station mounted above the deck.
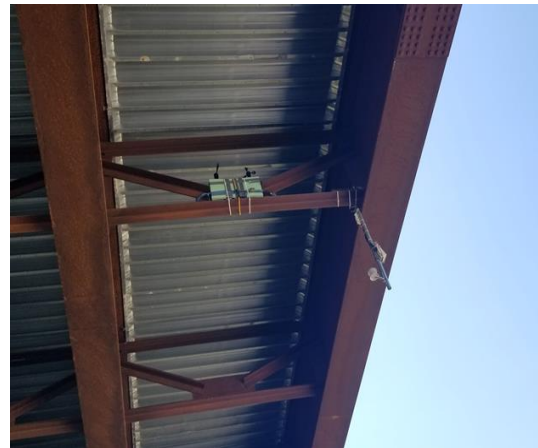
Figure 4.1: Location of wind speed and direction sensors within interior diaphragm at bridge. Note mast containing data acquisition/transmission equipment and temperature/humidity sensors mounted near

Only the average wind speed and the gust wind speed were analyzed in this project. The data collected above the bridge deck was compared to other four permanent weather stations located near the bridge. The weather station data was accessed through the WeatherUnderground website [65]. Figure 4.3 shows the average wind speed (a) and average gust (b) for the month of September. The Raleigh-Durham International (RDU) airport station best agrees with the bridge data.
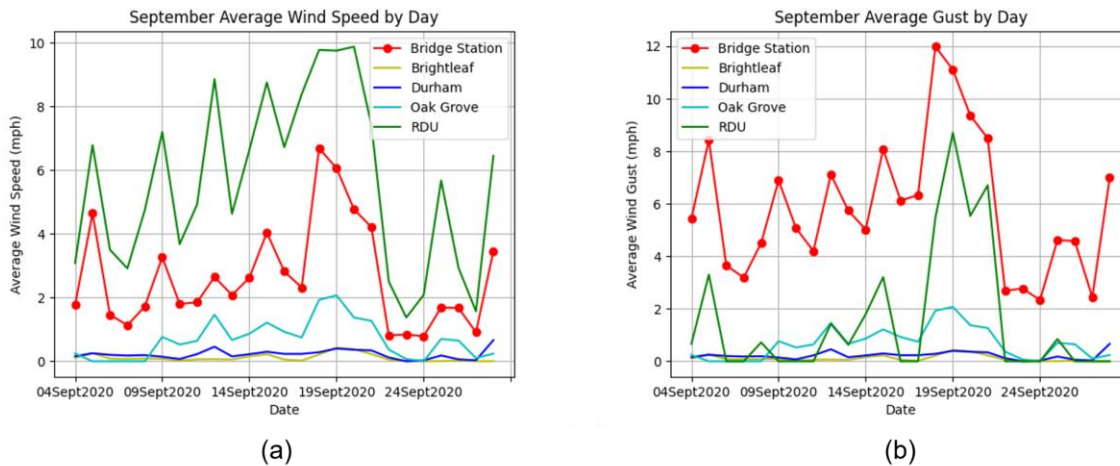
Figure 4.3 Wind speed (a) and wind gust (b) for the month of September 2020.

While the wind above the bridge can be estimated using an existing weather station. The under-bridge environment is most relevant to the UAV. This environment wass impacted by (1) the shielding provided by the bridge deck, (2) a channel effect provided by the roadway under the bridge and the end bent structures, and (3) the bridge components such as girders, and diaphragms. Likewise, the gust data has more value when trying to predict the environment and forces encountered by a UAV inspecting the bridge

structure. Figure 4.4 shows the gust data for both the RDU weather station and the below bridge deck data. Notice that the under-bridge data shows less variation in the wind speed (due to shielding) and lower magnitudes.
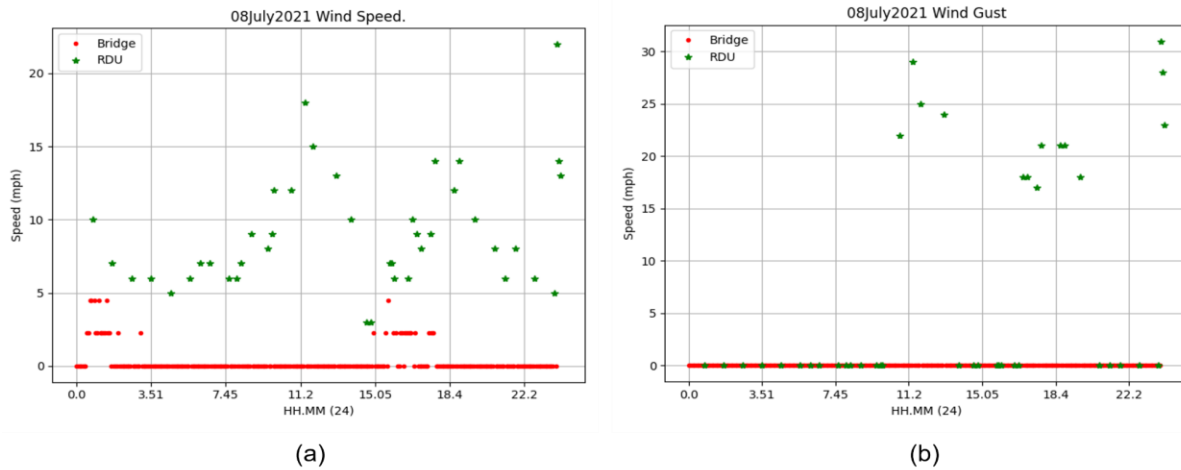
Figure 4.4: Wind speed (a) and wind gust (b) during Hurricane Elsa, July 8, 2021.

The resolution of the weather station was not high enough to capture the gusts near the under-deck bridge components. The impact of the resolution (2.5 mph) can be seen in the wind speed data as well. A summary of the weather conditions measured at the bridge is shown during Table 4.1 below. The average wind speed is below the resolution of the sensor and the average gust is near the resolution.

Table 4.1: Summary of weather station data.

	Wind Speed (mph)	**Wind Gust (mph)**
Above Bridge **Sept. 4 – Oct 1, 2020**	Max. 112 Avg. 2.6	Max. 22.5 Avg. 5.88
Below Bridge **May 10 – July 8, 2021**	Max. 13.4 Avg. 0.3	Max. 26.8 Avg. 3.4

The limitations of the weather station sensors and the lower than expected wind gusts experienced during the monitoring periods prevented the creation of transient boundary conditions for the CFD analysis. The data general boundary conditions both above and below the bridge.

4.3 CFD Methodology and Numerical Setup for UAV Flight Simulation

The goal of the CFD modeling section of this work was to analyze the aerodynamic performance of the Skydio 2 UAV unmanned aerial vehicle (UAV) as a supplementary tool for bridge girder inspections. In pursuit of this goal, this section of the present work presents aerodynamic performance evaluation results via computational fluid dynamics (CFD) of the Skydio 2 UAV for bridge girder inspection. The numerical predictions were performed using ANSYS FLUENT (v. 19). The CAD model was developed using MATLAB and Solidworks CAD software. Images were taken of the UAV 1 2 Drone used in the present work (shown in Figure 4.5) and were deployed to MATLAB software. MATLAB code was written to translate pixels to scale measurement increments based on the true scale of reference dimensions of the UAV. The computer aided design (CAD) model of the Skydio 2 UAV is shown below in Figure 4.6.
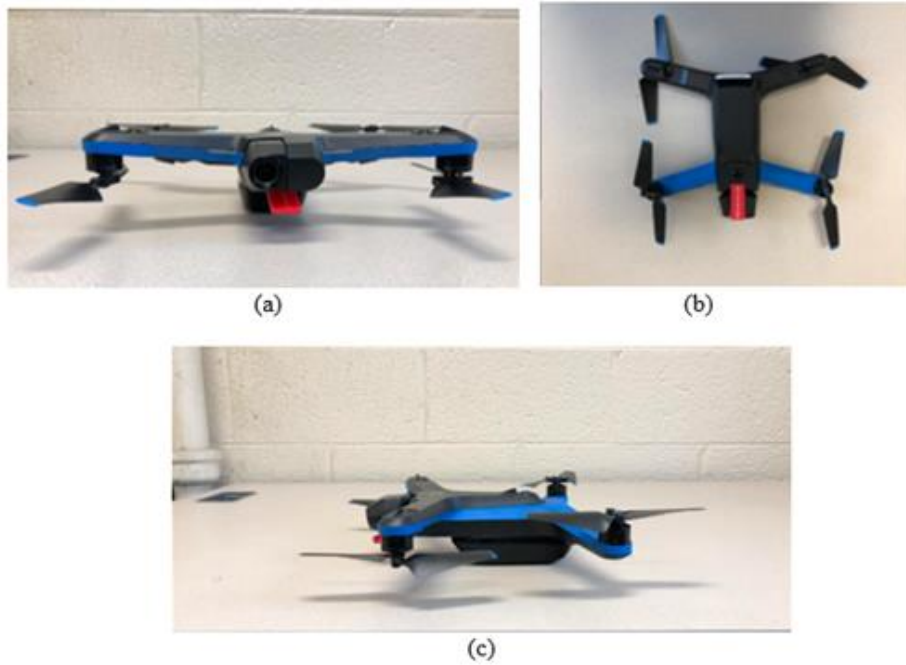
Figure 4.5: Photographs of the actual Skydio 2 UAV.

Figure 4.6: Developed Solidworks CAD model of the Skydio 2 UAV.

The CAD model was exported as a Parasolid file to ANSYS Design modeler where intricate parts of the model which would have a minimal effect on the fluid flow but would present issues for meshing were removed. Faces were also healed in sections where there are sharp edges.

The ANSYS FLUENT standard k-ε model was used to model fluid flow. The standard k-ε is a semi-empirical model based on model transport equations for the turbulence kinetic energy (κ) and its dissipation rate (ε). The model transport equation for κ is derived from the exact equation, while the model transport equation for ε was obtained using physical reasoning and bears little resemblance to its mathematically exact counterpart. The turbulence kinetic energy, κ, and its rate of dissipation, ε, are obtained from the following transport equations:

$$\frac{\partial}{\partial t}(\rho\kappa)+\frac{\partial}{\partial x_j}(\rho\kappa u_j)=\frac{\partial}{\partial x_j}\left[\left(\mu+\frac{\mu_t}{\sigma_\kappa}\right)\frac{\partial\kappa}{\partial x_j}\right]+G_\kappa+G_b-\rho_\varepsilon-Y_M \tag{1}$$

and

$$\frac{\partial}{\partial t}(\rho\varepsilon)+\frac{\partial}{\partial x_j}(\rho\varepsilon u_j)=\frac{\partial}{\partial x_j}\left[\left(\mu+\frac{\mu_t}{\sigma_\varepsilon}\right)\frac{\partial\varepsilon}{\partial x_j}\right]+\rho C_1 S_\varepsilon+-\rho C_2\frac{\varepsilon^2}{\kappa+\sqrt{v\varepsilon}}+C_{1\varepsilon}\frac{\varepsilon}{\kappa}C_{3\varepsilon}G_b \tag{2}$$

where

$$C_1=\max\left[0.43,\frac{\eta}{\eta+5}\right],\ \eta=S\frac{\kappa}{\varepsilon},\ G_\kappa=-\rho\overline{u_i'u_j'}\frac{\partial u_j}{\partial x_i}\ \text{and}\ S=\sqrt{2S_{ij}S_{ij}} \tag{3}$$

In the equations above, G_κ represents the generation of turbulence kinetic energy due to the mean velocity gradients calculated. G_b is the generation of turbulence kinetic energy due to buoyancy, and Y_M represents the contribution of the fluctuating dilation in compressible turbulence to the overall dissipation rate. C_2 and $C_{1\varepsilon}$ are constants and σ_κ and σ_ε are the turbulent Prandtl numbers for κ and ε respectively. The Multiple Reference Frame Model (MRF) approach was also used to numerically predict flow around the propellers of the UAV model. The MRF model is a steady-state approximation in which individual cell zones can be assigned different rotational and/or translational speeds. The flow in each moving cell zone is solved using the moving reference frame. Further information on this model can be found in the ANSYS FLUENT User's Guide.

4.4 Flow Domain

The meshed fluid flow domain is defined and illustrated in Figure 4.7 (a). The domain is split into a global stationary domain and subdivided into four rotating domains. The rotating domains are defined by a small cylinder enclosing the blades as shown in Figure 4.7 (b) (yellow meshed regions). The inlet, outlet, and surrounding faces of the stationary region are dimensioned at a length of to accommodate the full development of the upstream and downstream flow from affecting the results for the analysis. The inlet and outlet boundaries are located both upstream and downstream from the centroid of the UAV body as shown in Figure 4.7 (c).

The mesh was generated using ANSYS meshing software. The quality of the computational mesh directly influences the results in terms of the rate of convergence and grid independence. For the present work, the cell sizes of the mesh were generated using a face sizing and tetrahedral meshing scheme unstructured in both stationary and dynamic (rotating) regimes. The selection is based on the rationalizations that unstructured tetrahedral grids have the capabilities to discretize complex geometries with fast and minimum user intervention. For grid independence, the first mesh was generated with a minimum face size of 0.004m and decreased in length scale increments of 20% until the delta change in terms of comparing current to previous mesh parametric results *(analyzing total pressure, wall shear, and vorticity)* were minimized to less than five percent error. Table 4.1 provides details for the final grid generation at which grid independence was achieved.
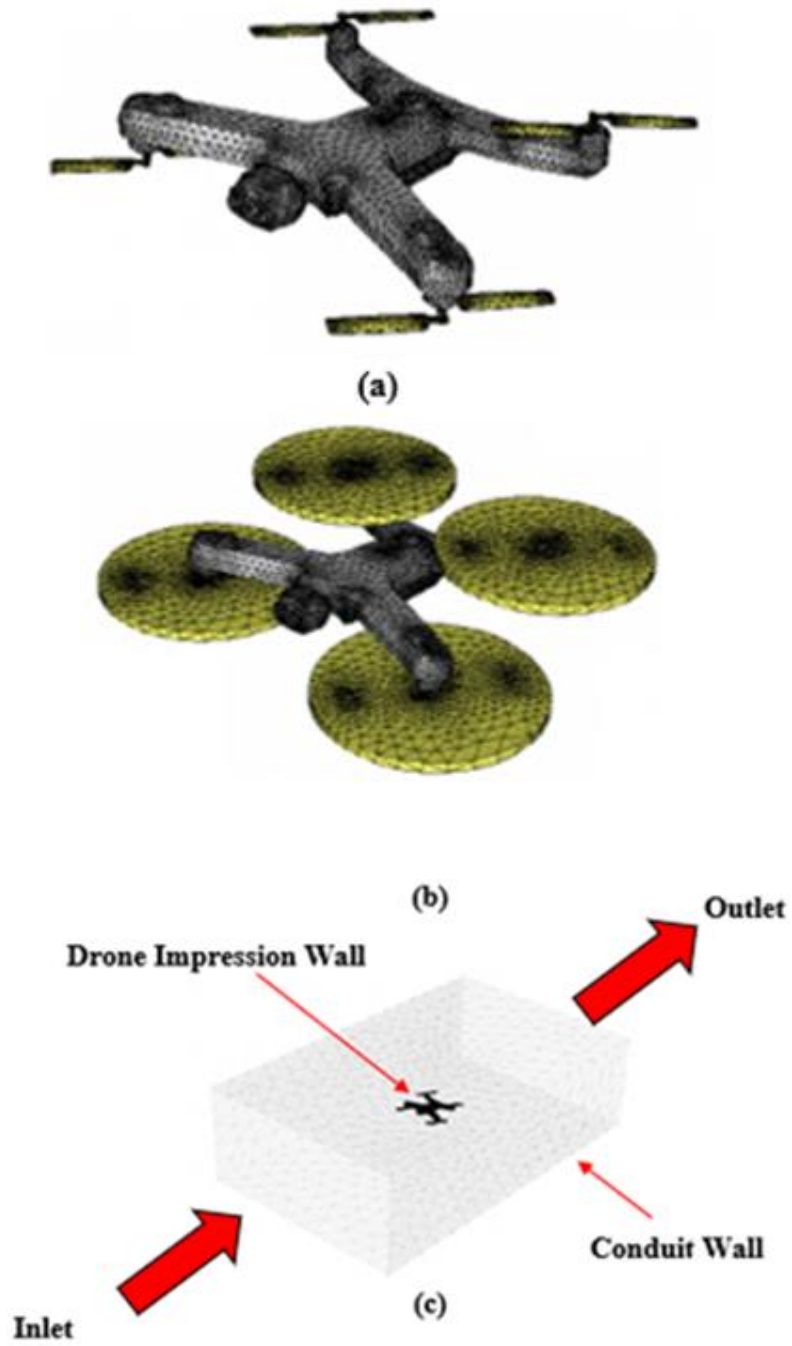
Figure 4.7. Fluid flow domain: (a) meshed drone body wall (b) UAV wall and rotating domains, and (c) global stationary region enclosed around the UAV and rotating domains.

Table 1: Details of mesh.

Size Function Parameter	Curvature
Relevance Centre	Fine
Curvature Normal Angle	40.7°
Min Size	1×10^{-4} m
Max Face Size	5.6718×10^{-2} m
Max Size	0.113440 m
Growth Rate	1.2
Minimum Edge Length	3.9199×10^{-6} m
Defeature size	1×10^{-8} m

Figure 4.8 shows the coarse mesh version of the surface and volumetric mesh of the propeller blade and rotating domain. A much finer mesh was used for running the simulations after grid independence was achieved.
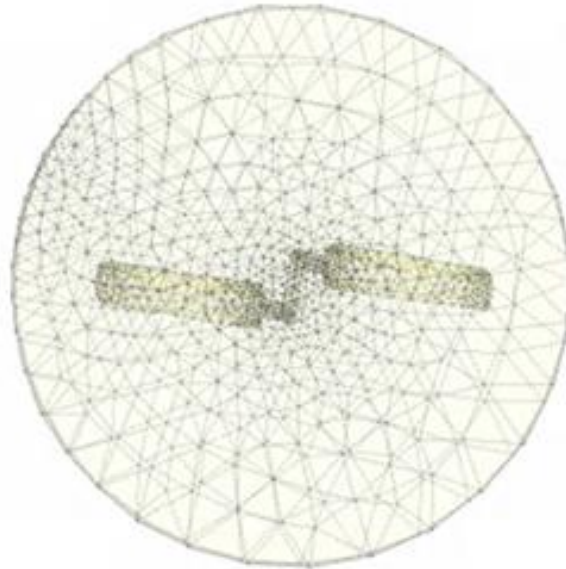
Figure 4.8: Coarse mesh of rotating domain enclosing the propeller.

The boundary conditions imposed on the model are summarized in Figure 4.7. At the inlet boundary, the free-stream velocity averaged around 1 m/s with a turbulence intensity of 0.1%. The turbulence intensity was set based on the wind tunnel intensity measured in references [66, 67]. A pressure outlet boundary condition was set at the flow exit downstream of the flow domain as shown in Figure 4.7. A no-slip condition is set on all the walls *(remaining conduit wall faces, drone body faces, and propeller faces).*

The domain that enclosed the propeller blade was assigned with the MRF to incorporate the rotational speed. The method is highly fitting for the analysis, which requires the interaction between stationary and rotating regimes. The individual zones were assigned with discrete rotational or translational speed. The interface needed between the two zones undergo a local frame transformation to enable the flow variable from one zone to be used by the adjacent zones. The moving reference frame was assigned with a rotational speed of 6000 RPM. The wall forming the propeller blade and the hub were also assigned as rotational, with a velocity of zero with respect to the adjacent cell zone. The pressure–velocity coupling was selected using a Semi-Implicit Method for Pressure-Linked Equations (SIMPLE). The Second Order Upwind scheme was used for momentum and pressure. The First Order Upwind for both Turbulent Kinetic Energy

and Turbulent Dissipation Rate and the Least Square Cell-based Algorithm were used for the gradients. The time step sizes used for transient analysis was set to 0.00015s.

For all CFD simulation analyses, the force and momentum were resolved in a three-coordinate system (x, y, and z). The axial force and momentum around the propeller axis define the thrust and torque, respectively. The total pressure is also calculated and defined as:

$$P_{Total} = P_{Static} + P_{Dynamic} + P_{Absolute} \tag{7}$$

Figure 4.9 provides a plot of the velocity vector and contour plots. As mentioned previously, the velocity of air flow from the inlet of the global stationary domain was 1 m/s. From Figure 4.9 (a)., the highest velocity magnitudes of flow occur around the tips of the rotating propellers (16.1 m/s). This suggested the flow is increased by high levels of thrust and lift forces produced by the torque output of the propellers. This is evident as shown in the contour plot in Figure 4.9 (b).
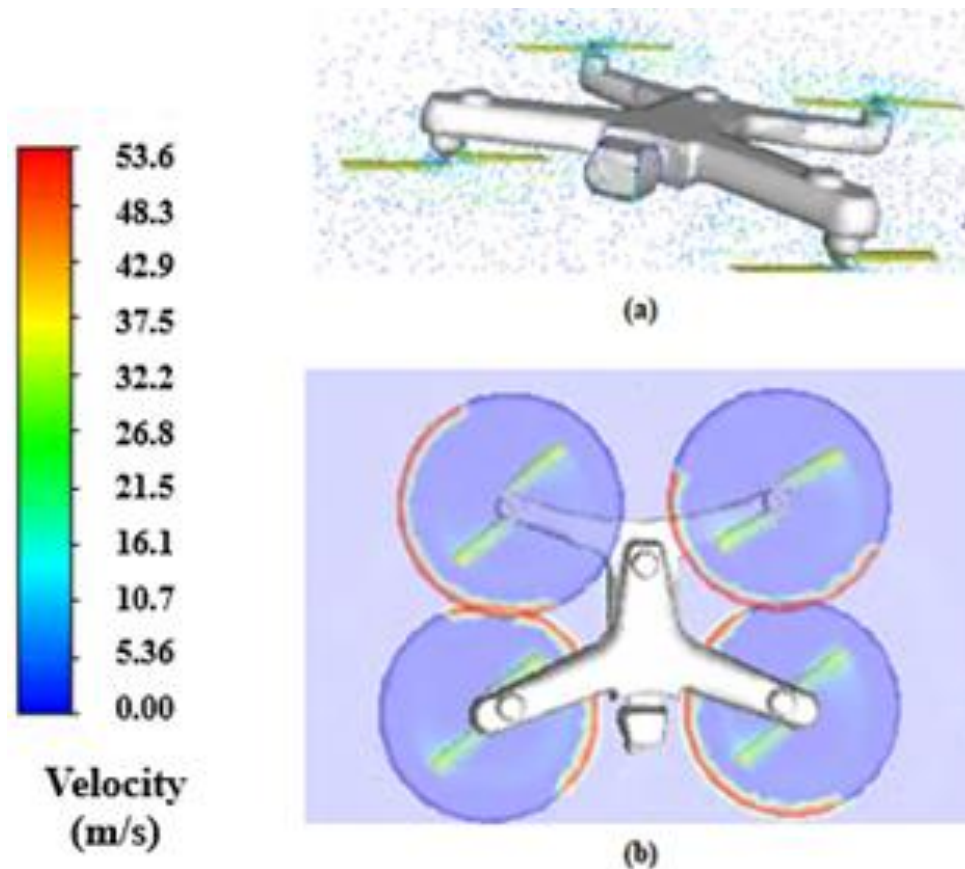
Figure 4.9: Velocity plots: (a) vector plots around rotating domains and (b) top view of UAV and velocity contours of rotating domains.

The red regions suggest that high levels of torque were produced that forces the flow outward of the rotating domains (high velocity regions highlighted in red). Figure 4.10 shows the total pressure contours around the drone body and rotating domains at 0.015s. The total pressure ranges from -61.8 Pa to 46.8 Pa. The pressure was negative because the pressure gradient drived the flow from high pressure regions to low pressure regions. Also, in the case of regions where there is flow separation, the low pressure inside that region will be relative to the lowest fixed pressure and can result in negative pressure. For the

propellers, the pressure difference between the front and back sides of the propellers createed a force in the forward direction resulting in thrust which made the UAV fly. In the case of the UAV body the pressure was near constant value around the body of the drone and showed higher pressure values near the tip of the propeller blades.
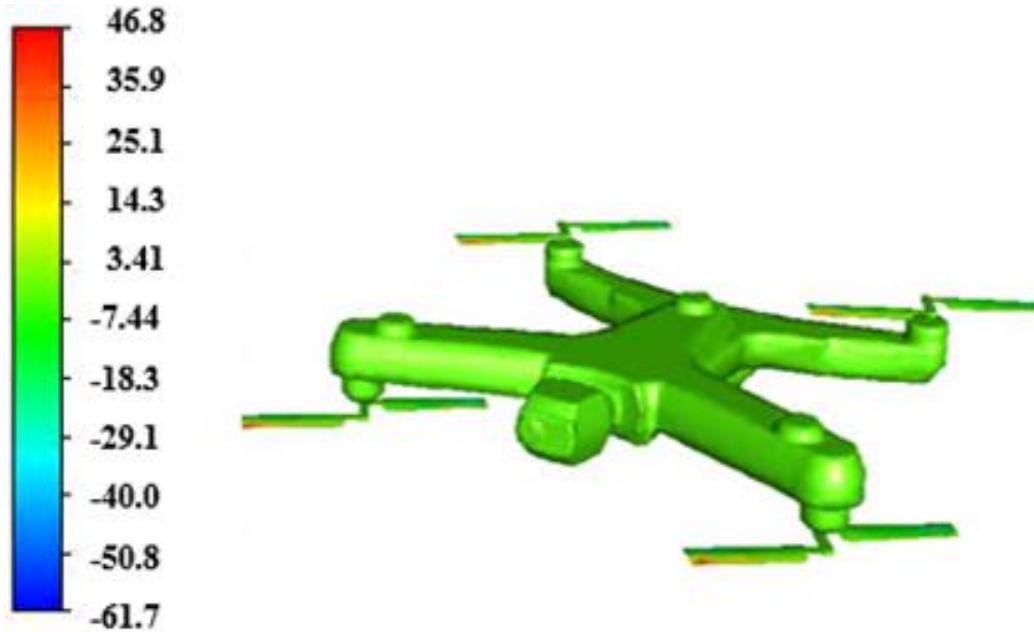
Figure 4.10: Total Pressure at time 0.0015s
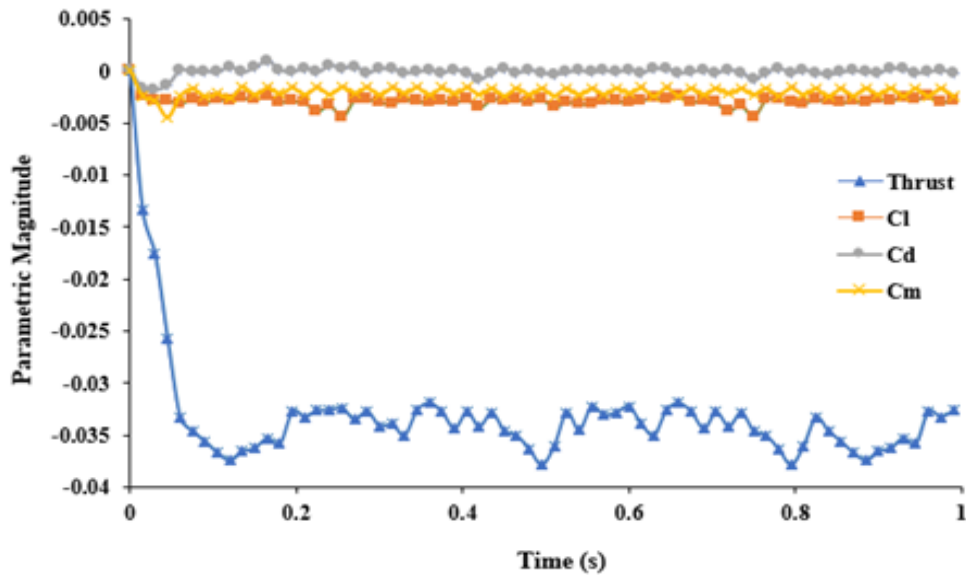
Figure 4.11: Plot of propeller performance parameters.

A better representation of the performance of the UAV can be found by analyzing the moment coefficient (torque), drag coefficient (C_d) coefficient (C_m), lift coefficient (C_l), and thrust force magnitude. Figure 4.11 presents a plot of these parametric results. All of these parameters were averaged over all four of the propellers of the Skydio 2 UAV. As shown in Figure 4.9., the

27

maximum thrust averaged around 0.035N. The maximum C_d, C_l, C_m, and C_d, averaged around -0.00013, -0.00292, -0.03312, and -0.00202. The values of these coefficients and force magnitude show indication that the UAV is suitable for flying in the given conditions. However, more simulation data is needed such as varying inlet boundary condition velocity magnitudes to show flight conditions in windy scenarios that would make bridge inspections difficult if not impossible.

4.5 CFD Methodology and Numerical Setup for Near-field Bridge Environment

A computational model of the bridge on US 70 Eastbound (structure 4) over the East End Connector in Durham, NC bridge was created in SolidWorks, Figure 4.12. (a) shows the entire bridge model. Figure 4.12. (b) shows the view of the understructure including the girders, diaphragms, and center support. Figure 4.12. (c) shows the end bent and Figure 4.12. (d) shows the pot bearing.

(a)

(b)

(c)

(d)
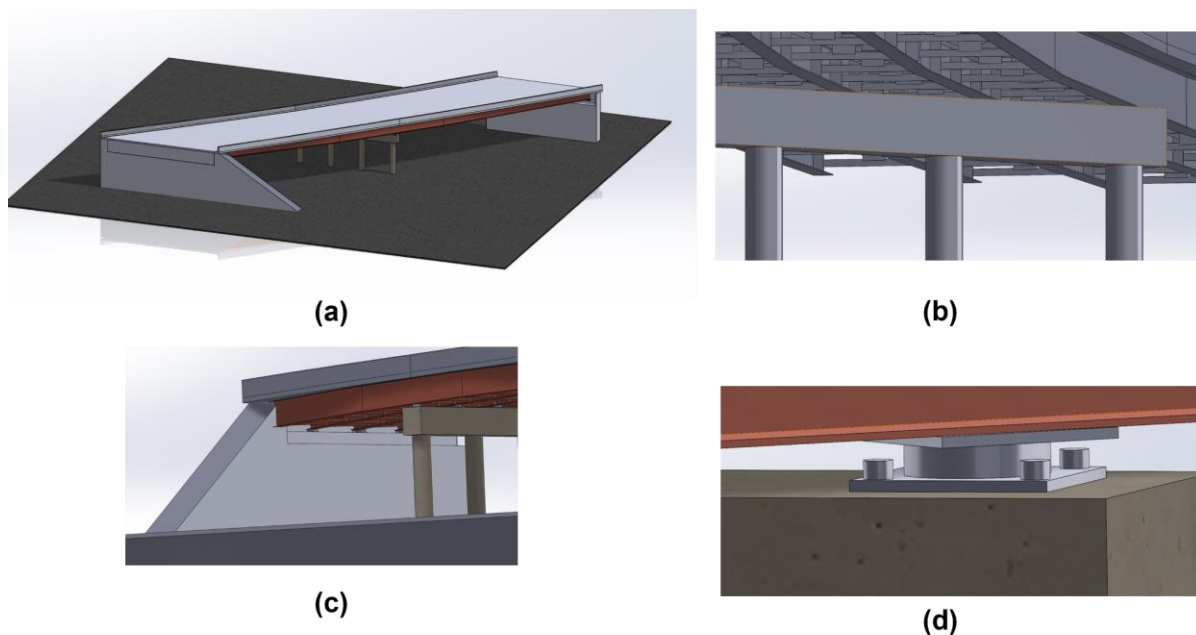
Figure 4.12: Solid model of structure 4.

To create a model that could be used in the CFD analysis the following simplifications were applied:

- The bolts, welds, and fasteners were not included.
- The girders were treated as continuous, i.e. the splices were ignored.
- Concrete joints were ignored. This applied to the bridge deck and concrete barriers.
- The corrugated metal under the bridge deck was not included.

The area between two girders with a series of three diaphragms was analyzed. The girder surfaces and the underside of the bridge deck are treated as solid walls. A constant velocity inlet condition was specified, and air exited through the end of the channel and the lower face. The entrance region from the inlet to the first diaphragm is 8 ft. The space between the diaphragms is 13 ft. which is the distance near the end bents of the actual bridge. This spacing provided the most cumulative effect. The diaphragm ended 20 inches above the bottom surface of the computational domain.

The computational grid consisted of 3,728,857 elements. A transient, turbulent calculation was

performed with a timestep of 0.01 seconds. The inlet velocity was 2 m/s or 4.5 mph. This velocity was slightly higher than the average gust velocity but less than the maximum values measured by the weather station when positioned under the bridge deck. The presented results are shown at a simulation time of 4 seconds.

Figure 4.13. shows the velocity contours through the series of diaphragms. Planes perpendicular to the diaphragms were used to display the fluid behavior. The first plane (left) is at the center point and the second plane (right) centered between the middle and wall. The second position is referred to as the quarter plane. This center position gives the best view of the jet that was formed through the large opening and the shielding provided by the gusset plate. The second plane best shows the flow disruption by the elements in the diaphragms.
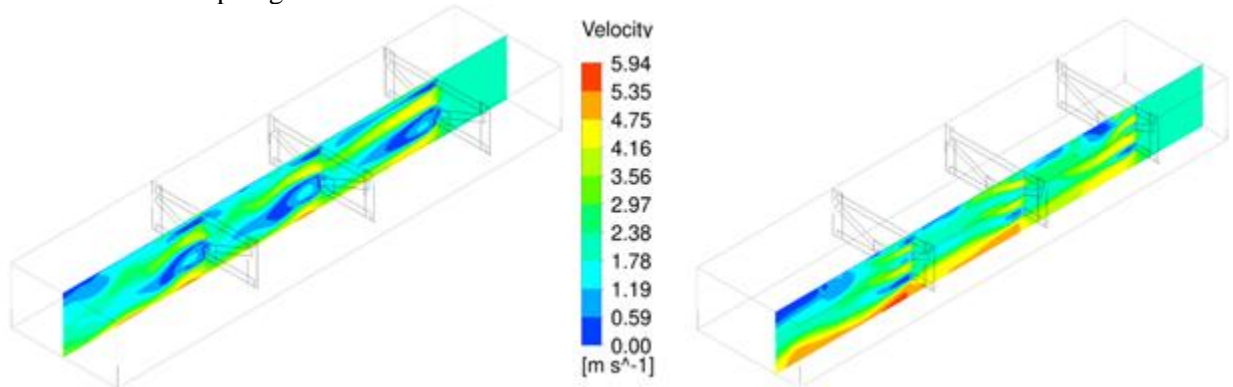
Figure 4.13: Velocity contours through a series of diaphragms along the center (left image) and the quarter plane (right image) with the bridge geometry.

The velocity along the long planes is presented below. The center plane shows the higher velocity jet that forms through the opening above the gusset plate. Notice that the jet becomes less defined in the second and third diaphragms. This is because the flow encountering the diaphragm is not a uniform, fully developed flow pattern. The shielded region below the jet also becomes less defined. The quarter plan shows less defined flow patterns.
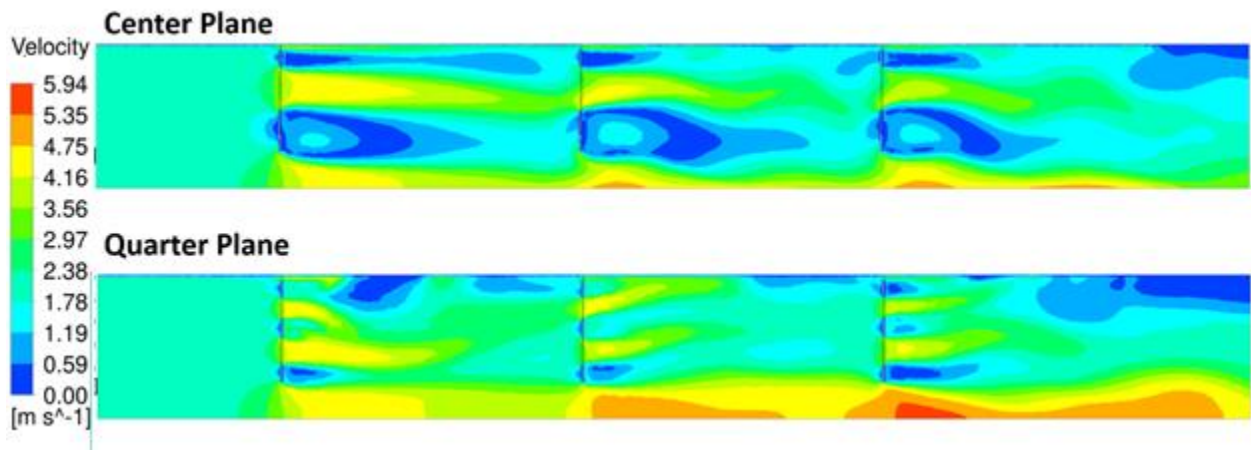
Figure 4.14 Velocity contours through a series of diaphragms along the center (left image) and the maximum velocity (right image).

The turbulence kinetic energy is shown on the two planes, Figure 4.15. The highest turbulence energy can be seen on the quarter plane in the region where the multiple fluid streams are remixing behind the diaphragm.
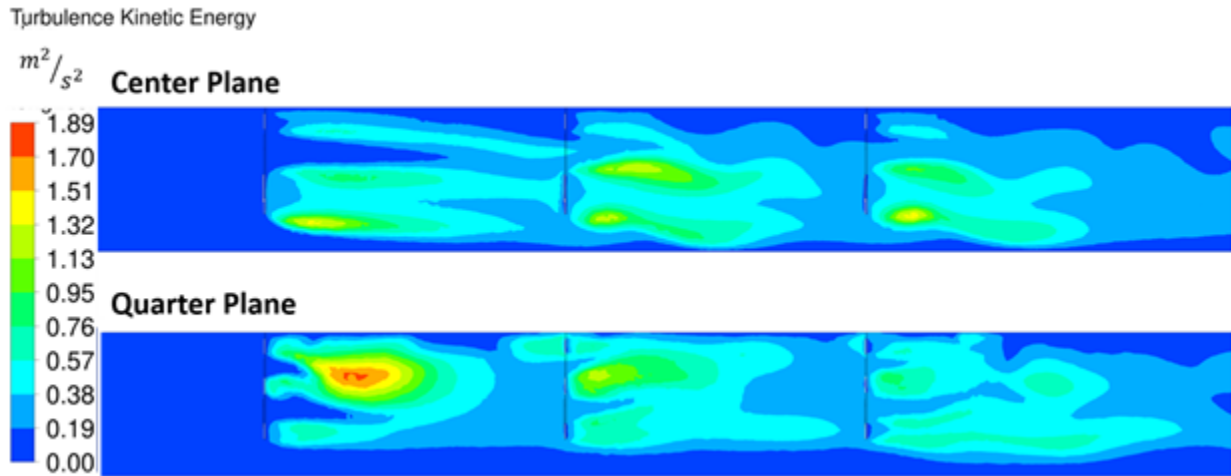
Figure 4.15 Turbulence kinetic energy contours through a series of diaphragms along the center (left image) and the maximum velocity (right image).

Views perpendicular to the plane above are also shown. Below are the velocity contours on planes 6 inched behind each of the three diaphragms. The inlet is to the right in the image. The effects of the diaphragm elements in the flow patterns are clearly seen in Figure 4.16.
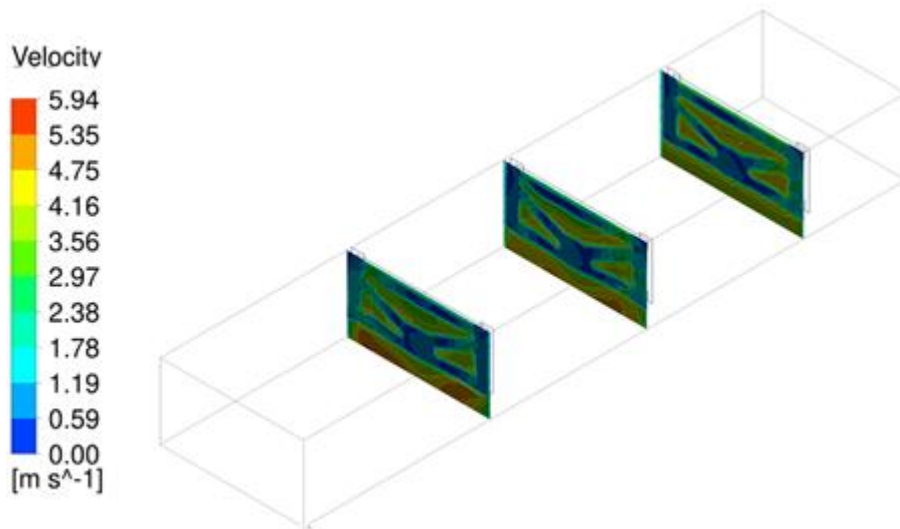
Figure 4.16: Velocity contours through a series of parallel to the diaphragms.

A series of the positions behind the first diaphragm are compared. The first was located 6 inches behind the diaphragm, the second at the mid-point, 6.75 ft, and third is 6 inches before the second diaphragm. By the final image the flow is becoming more uniform with the impact of the wall friction still evident.
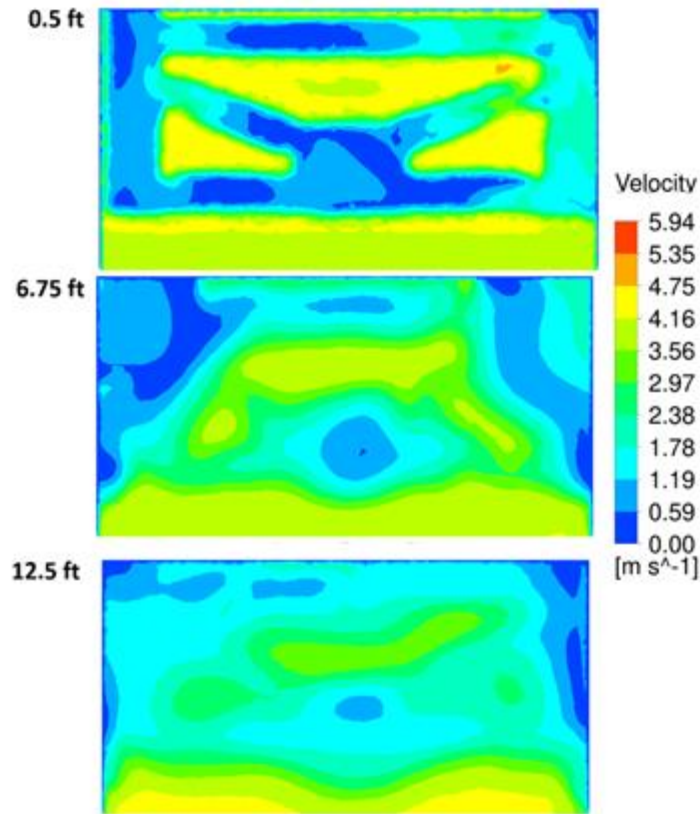
Figure 4.17: Velocity contours with increasing distance from the diaphragm.

4.6 Summary of findings

The parametric results for the Skydio CFD studies show reliable moment coefficient and thrust making the Skydio 2 UAV suitable for bridge inspection in low wind (1 m/s) conditions. A second simulation was run on a model of the bridge on US 70 Eastbound (structure 4) over the East End Connector in Durham, NC bridge with a varying inlet velocity. Data from this simulation is essential to show flight conditions in windy scenarios that would make bridge inspections difficult if not impossible. The results presented from the bridge model studies show high levels of unsteadiness throughout the diaphragm and areas low to the ground. These are regions where the highest levels of fluid energy losses and high circulation would occur and make flight difficult during high wind scenarios (wind speeds greater than 1 m/s). It appears that the highest flow recirculation zones occur near the entrance region and dampen with distance. The velocity magnitude decreases, but recirculation patterns continue as a cause of acceleration and deceleration of air due to cross-sectional changes and variations in the flow conduit (area under the bridge). These are the regions where flight would be difficult due to flow recirculation and wakes. Future work is needed where the UAV and the bridge is modeled together to show the level of fluid forces acting on the UAV as a function of inlet velocity conditions.

5   DESIGNING EXPERIMENTS TO TEST AND EVALUATE THE PERFORMANCE OF THE UAVS FOR BRIDGE INSPECTION

5.1 Introduction

The first part of this chapter discusses UAV features the research team deemed important for bridge inspections. The various criteria under each category were reviewed, with respect to how each criterion can affect bridge inspection tasks. Some of these features are provided in the manufacturers specification document and thus were retrieved from manufacturer's published literature. In addition, the research team designed different experiments for the evaluation of UAV capabilities that are important for bridge inspection. In this section, different experiments will be presented for testing various capabilities of UAVs.

5.2 Experiment Design Process

The test and evaluation experiment design process follows a well-established scientific method. It is a systematic and straight forward approach that includes the problem definition, objective establishment, articles of experiment selection, experiment execution, verification of results consistency and conclusion.
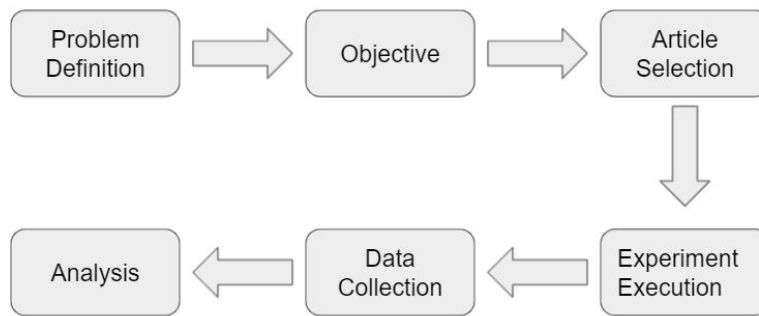
Figure 5.1: Experiment design process.

The problem definition stage set out clearly the desired goal of the experiment. This stage also involves identifying all response variables for the device under test (DUT). In the current work, the responsible variables were identified using a combination of literature and advice from experts in infrastructure inspection. The response variables deemed critical for bridge inspection are flight performance, situational awareness, communication and payload. Each of these variables/categories have sub-variables or criteria as indicated in Table 4.1 These sub variables are the key process input variables that will be tested and evaluated. The second stage of the experiment design involves the establishment of the objective. This design stage involves outlining what is expected to be achieved with these experiments. In this work, some of the objectives aim to verify whether or not the DUT adheres to the specification information indicated in the specification documents. In other cases, the objective aimed to examine the response of the DUT under both normal and abnormal conditions. Following the objective definition, the articles of the experiments were identified. The article varied depending on the experiment but in all cases the UAV was part. For experiments that involved generating radio frequency (RF) signals, all regulatory rules regarding RF signal use to ensure other services are not impacted were adhered to. The final step involved experimental execution, data collection and results analysis. In most cases, subjective means to quantify the results of our analysis were used. However, where possible, quantitative analysis was performed.

5.3 RF Immunity Testing

UAVs are remotely piloted with the command-and-control signals, and the telemetry data as well the payload data is transmitted via RF channels [68, 69, 70]. The frequencies used by the command-and-control links of UAVs are typically in 72-73, 902-928 and 2400-2483.5 MHz bands [71], while the video transmissions are usually made via 5.2 GHz bands. These frequencies are not used solely by the UAVs.

There is a proliferation of services that use communication networks such as, WiFi, ZigBee, LTE, and GSM that operate on the same frequency bands. Therefore, there is a high chance for these services to impact the performance of UAVs particularly in environment where there is a proliferation of RF sources [72].

Federal Communication Commission (FCC) requires all electronic equipment including UAVs to meet a minimum Electromagnetic Compatibility (EMC). UAVs are usually manufactured for general-purpose use which is always governed by a trade-off between the performance and cost-effectiveness, and therefore, it is unlikely that the manufacturers will be able to handle all environmental conditions and maintain the EMC for all possible RF scenarios that a UAV may encounter during its operation.

Thus, in this section, the UAV's immunity to interference is investigated by designing and conducting the field experiments that can subject the UAVs to controlled electromagnetic interference and distortions that are usually encountered in a UAV-enabled bridge inspection environment. To achieve this goal, the subject UAV platforms were exposed to different levels of interference. It is followed by an analysis of how the presence of interference impacts the UAV's response to the controller's control commands. Finally, the impact of the RF stress on the transmission of telemetry data and payload (i.e., camera) data from the UAV to the controller is 30investigated. Here, only the RF immunity experiment is described. In chapter 4, the results are presented.

5.3.1   RF Immunity test setup

The main test articles for the RF immunity test are UAV's, Agilent N9310A RF signal generator and Agilent CXA 9000 signal analyzer. The experiment was conducted using three general-purpose UAVs. We compared the results of the three UAVs, UAV 1, UAV 2, UAV 3, UAV 4 and to determine the one with the strongest immunity to RF interference. The electromagnetic interference was created using Agilent N9310A signal generator. It supports frequencies in the range of 9kHz – 3GHz, and thus, its range covers the operating frequency for the UAV's communication channels as well as other RF signals that are likely to interfere with the UAV's channels. Furthermore, we used the Agilent CXA 9000 signal analyzer to measure the environmental average RF signal power levels, the UAV's Remote Command (RC) transmission power, and the interference generated by Agilent N9310A signal generator. It supported frequencies over the ranges of 700MHz - 3 GHz. The signal generator and analyzer were connected to a wide-band antenna that supports their respective frequencies. Figure 5.2. shows the setup used for conducting the tests. Since this experiment involved RF interference generation, it was carried out in accordance with the Federal Aviation Authority (FAA) and the Federal Communication Commission (FCC) regulations. The tests were conducted away from commercial radio, TV antennas, and FAA or military radars to ensure that the tests did not impact their services.

Figure 5.2: RF test setup.

5.3.2 Test procedure

As an initial step, the frequency range of 2 to3GHz was scanned to establish the environment's RF signal power using RF Signal Analyzer. The UAV and controller/controller were then turned on. The UAV was then positioned initially at approximately 1m from the signal generator. At this point, no interference was observed. The status of the RF and video feed was checked, in addition to all other information discussed above, to ensure that the UAV is operating as expected. The UAV was then moving away from the interference source at discrete steps. The impact of the interference on GPS signal, video feed, command and control signal was then observed.
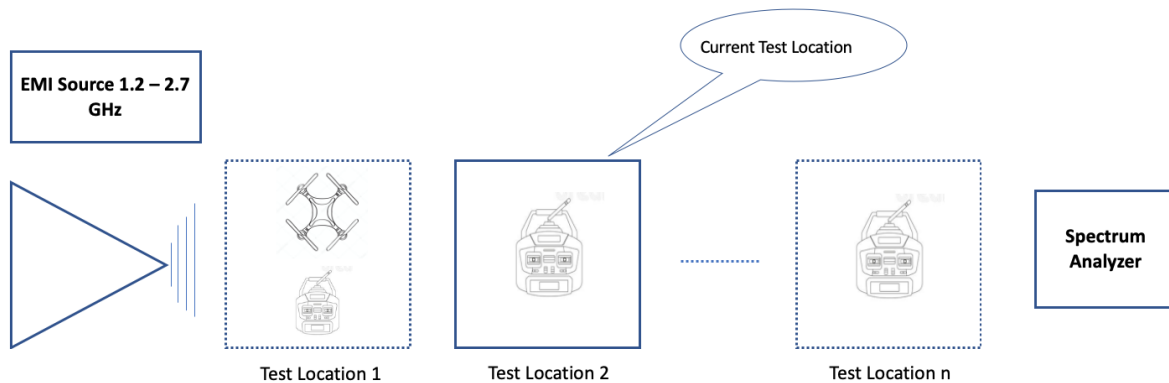
Figure 5.3: Pictorial view of RF experiment

5.4 Endurance Testing

Endurance testing provided an indication of the maximum flight time that can be achieved with a fully charged battery. The testing of this operational criterion is important because bridge inspection can take hours, days, or weeks (for long bridges such as the Virginia Dare Bridge) to complete depending on the nature of inspection i.e., in-depth inspection or routine inspection. While a UAV with limited flight time may suffice in inspection tasks such as in-depth inspection of specific superstructure and substructure elements or appurtenances, it may not be appropriate for bridge deck inspection. Therefore, it is important to evaluate the endurance to identify the most appropriate platform for a particular situation. Although the battery time is usually listed in the manufacturer's specification document, that value indicates hovering mode endurance. In bridge inspection, usually the UAVs will be used in forward mode, thus this test is important to determine the true battery life of the respective UAVs.

5.5 Endurance test setup

The test setup of endurance included all the three UAVs mentioned in the previous section. A stopwatch was used to keep track of how long the UAVs battery last. For all the UAVs, the amount of time it took for the battery to drop 25 % of its capacity was recorded. For UAVs with auto-land feature, the research team also recorded the time it took to initiate auto-landing. The experiment was executed in both hovering and forward mode.

5.6 Hovering mode endurance test procedure

1. Equip the UAS platform with fully charged batteries.
2. Take off from a suitable location and hover the UAV at a certain altitude.
3. Fly the UAS in hovering mode until reaching 20\% of the battery level.
4. Record the flight time.
5. Continuing flying until low-battery alarm is activated or auto-landing initiated.
6. Record the flight time.
7. Land the UAS.
8. Repeat the above process for 3 times and take the average flight time in both cases.

5.7 Forward mode endurance test procedure

1. Equip the UAS platform with fully charged batteries.
2. Plan and load a mission onto the UAS memory device (applicable to UAS that support this feature).
3. Continuing a fixed linear path flying until low-battery alarm is activated or auto-landing initiated. The same path was used for all UAVs.
4. Record the flight time.
5. Land the UAS.
6. Repeat the above process for 3 times and take the average flight time in both cases.

5.8 Vibration Testing

Rotor and gimbal vibration can introduce noise to images captured with UAVs [73, 74] and may subsequently affect the effectiveness of algorithms used for post-processing of the images. Depending on the quality of the UAVs gimbal's controller, the vibration impact will be different. Therefore, our objective was to design an experiment to test the UAS's capability of handling vibration effects on image quality. This was achieved by comparing successive images taken in a short time with the UAV in hovering mode. he peak signal to noise ratio (PSNR) of each image against a reference image was computed using the equations below.

$$PSNR = 10log\frac{MAX_i}{\sqrt{MSE}}$$

$$MSE = \frac{1}{row*col}\sum_{i=0}^{row-1}\sum_{j=0}^{col-1}||Image_{ref}(i,j) - Image_{test}(i,j)||$$

Here, the first captured image is used as the reference image. In an ideal situation where vibration has no impact on the image quality, it could be expected that the PSNR would be zero since all the images will be the same.

For an example, consider a 25-pixel reference and test image shown in Figure 5.4. Here, row=5 and col=5. MSE is computed by first finding the difference between corresponding pixel values in both reference and test images. The norm of the difference is computed and then divided by the resolution of the image. MAX_i depends on the number of bits used to represent each pixel. If 32 bits are used $MAX_i = 2^{32-1}$
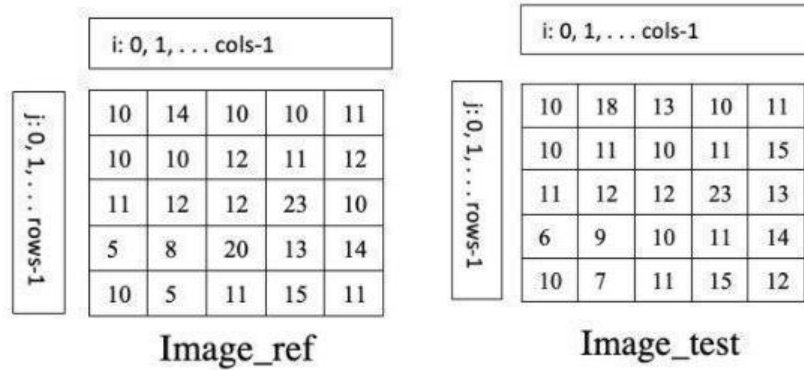
Figure 5.4: A 25-pixel image.

5.8.1 Vibration Test Setup

The test articles for vibration testing included the 3 UAVs platform and a test element. The different UAVs were used to capture successive images of the test element. The first image was considered to be the reference image and subsequent images as test images.

5.8.2 Vibration Test Procedure

1. Attach a test element with a known and visible defect onto a section of the bridge's upper deck.
2. Take-off and fly to a suitable altitude
3. Set the UAV into hovering mode if it has this functionality.
4. Take two images of the test elements at intervals of about 1 seconds.
5. Repeat the previous step an arbitrary number of times.
6. Compute the PSNR between the first captured image and the second image using the equation above.

5.9 Global Position System (GPS) Testing

GPS signals around bridge infrastructure are usually unstable, and as such, there is a likelihood of GPS signal loss during inspections especially at the underside of the bridge deck. This can result in UAV crashes

especially when operating in GPS mode [75]. It is also known that electromagnetic interference can impact the reliability of the GPS signals. Therefore, to ensure an accident-free bridge inspection, there is a need to evaluate the reliability of the GPS of the platform which is selected for bridge inspection to provide a safe performance. In this work, the time it takes for the GPS to recover when there is an abrupt loss in GPS signal was evaluated. This is called the Time-to-recover.

5.9.1   GPS test setup

The test articles for GPS testing comprise of the 3 UAV platforms, a stopwatch and an aluminum metal shield. Aluminum is known to obstruct GPS signals thus we used it to simulate GPS denied environments likely to be encountered by the UAVs when operating under the bridge deck. The test was set up in open space where the GPS signal is known to be very good. Figure 5.5. shows the initial setup of the test. At this point we have allowed the UAV to establish full GPS connection. The final stage of the test, where the UAV was covered with the aluminum shield to block the GPS signal is also shown in Figure 5.6.

Figure 5.6:: GPS test setup: initial state.

Figure 5.5: GPS test setup: final state.

5.9.2   GPS test procedure

1. Turn on the platform and wait until the GPS status changes from "searching" to "OK" or GPS signal passes the initial oscillations and reaches a stable situation.
2. Cover the UAS with a metal shield for about two minutes, to deny the GPS signal.
3. Remove the metal shield and observe the time it takes for the GPS status to change from "searching" to "OK" GPS signal passes the initial oscillations and reaches a stable situation.
4. Record the time using the stopwatch.
5. Repeat the above procedure for 10 times and then find the average.

5.10   Illumination Testing

The level of illumination under bridges can greatly impact the quality of images taken with the camera mounted on the UAV. The illumination level becomes crucial when inspecting components of the bridge under the deck. Aside from the natural illumination provided by the sun, most UAVs are equipped with LEDs to provide some form of illumination during the inspection. This can be checked by visual inspection. However, it is important to evaluate the performance of the payload camera when used to capture images at different times of the day. This test was conducted inside a room with variable lightning control. A sample test piece with the UAV was examined under different lighting conditions, to observe how the reduced lighting impacted the ability of the UAV to detect defects in the test piece.

5.10.1 Illumination test setup

The main articles for the illumination test included 2 UAVs, a mobile phone with light-meter installed, test element (with known defects) and a room with variable lightning control. The test element used was a concrete block with some defects. Figure 5.7 shows the test element on a stand inside the test room. The background of the test room was chosen to provide good contrast in color. The different illumination levels were estimated using the light-meter. Although the light-meter may not be the most accurate illumination measurement tool, it has been shown to provide reasonable values within the lux range used for conducting this experiment [76]. Four different lightning conditions were considered to simulate the illumination scenario that is likely to be encountered during bridge inspection. These are:

- Level 1 (Dark): 10 - 130 lx
- Level 2 (Intermediate 1): 130 - 220 lx
- Level 3 (Intermediate 2): 220 - 250 lx
- Level 4 (Bright): above 250 lx

Figure 5.7. Illumination test setup.

5.10.2 Image Quality Assessment

Although we can visually determine which UAV camera performs best, we computed the entropy of each image using the equation below.

$$H(x) = \sum_{i=1}^{n} p_i log_2 p_i$$

Here, p_i value is the occurrence probability of a given symbol. For images, the symbols are the pixels. Entropy is a statistical measure that gives an indication of the average information content in an image. It depicts the information content in the aggregated features of the grayscale image. The research team's assumption was that if the image has a high quality and sharp enough to enable detection of defects, then its entropy should be higher. This metric makes comparison between the images captured by the different UAVs straightforward and eliminates human bias in interpretation.

5.10.3 Illumination test procedure

1. Turn on the UAV and camera.
2. Initially, set the illumination in the test room to level 1.
3. Position the test element at 60 cm from the UAV.
4. Inspected and captured images of the test element with UAV's camera.
5. Repeat steps 3 and 4 using lightning levels 2 to 4.
6. Repeat the above for all three UAVs.
7. Repeat the above using 120 cm for step 3.

5.11 Autonomy Testing

The autonomy testing evaluated the capability of the UAVs to execute planned missions as well as the capability of execution of safety features for managing emergency situations. The research team considered UAVs that have support for autonomous waypoint following, auto landing, and return to home functions. These autonomous functionalities can be crucial for safe bridge inspections. For instance, the UAVs can be programmed to return to home, when there is a communication link loss between the UAVs and the controller to avoid crashing. In addition, the inspection of the bridge facade and upper deck can be achieved by loading a planned mission on the UAVs for autonomous inspection. This reduces the human factors' influence in the inspection process, and thus reduces accidents and improves efficiency. In the following section, the tests for waypoint following, return-to-home, and lost-link recovery are described.

5.11.1 Autonomy Test Setup

The main articles for these experiments are the UAV platform. This test was carried out on a large football field. A sample mission that took approximately 10 minutes was planned, using third-party software. Three different functionalities were examined under autonomy. These are autonomous waypoint following, auto landing, and return to home functions. Before flying, "return to home" was activated for UAVs that support this feature.

5.11.2 Autonomous waypoint-following procedure

1. Load a planned mission onto the UAV's memory device (applicable to UAVs that support this feature).
2. Take off and allow the UAS to fly autonomously following the waypoints of the loaded mission.
3. When the mission is complete, land the UAV.

5.11.3 Auto-land procedure

1. Take off and fly the UAV in a suitable area.
2. Continue flying following mission's waypoints until auto-landing is activated (for supported UAVs)
3. Allow the UAV to land itself.

5.11.4 Return to Home Test Procedure

1. Take off and fly the UAV in a wide open area.
2. In the middle of the mission, turn off the controller/RC to enable the lost-link recovery process if it is safe to test.

5.12 Maneuverability Testing

The inspection of certain bridge components may require the UAV to navigate through confined spaces. For instance, the inspection of the steel/concrete box girders, steel arch rings, arch tie girders and some bearing types, etc. may require the UAS to perform a range of maneuvers in confined spaces. Furthermore, the inspection of bridges of many types (such as steel truss) or configurations will typically require flying the UAS between the members in order to reach certain components of the bridges. Thus, there is a need to test the maneuverability of candidate UAS platforms to identify platforms that can perform well in the bridge inspection scenarios.

5.12.1 Maneuverability Test Setup

The scope of this test was limited to testing and evaluating confined space navigation and agility. The main articles for the experiment were 3 UAV platforms. The exit criteria for this experiment is successful navigation in confined bridge areas. The main idea of this test is to examine how easily the candidate UAVs can navigate around obstacles to carry out inspection.

5.12.2 Maneuverability Test Procedure

1. Select a suitable bridge for testing.
2. Take-off and fly towards the bridge.
3. Navigate through the concrete piers while inspecting the underside of the bridge deck.
4. Observe the ease with which each UAV and its capability to navigate its way through the piers.

5.13 Agility Testing

Agility is another criterion that is worthy of testing due to its importance to bridge inspection. It gives an indication of how quickly a UAV's flight path can be altered when commanded to do so. In other words, it is the measure of the maximum possible rate of change of the acceleration vector at any point in the flight envelope [77]. The higher agility, the better the UAS can withstand turbulence and gusts. This becomes particularly important when the UAS is used for close-range inspections in confined areas likely to be encountered in bridge inspection. Therefore, in this experiment, the UAV's time constant in different channels was measured as an index for the response time and agility of the platform. The time constant, τ, is characterizing the response time to a step input. A UAV with a shorter time constant responds quickly to input change whereas, a UAV with a long time constant behaves sluggishly. To be able to generate a constant input into the input channels, we require the RC control rods to push to the maximum, and hence, a large test field is needed to allow execution of this test.

5.13.1 Agility Test setup

The scope of this test was limited to the response of the UAV to issue commands from the controller. The main articles for the experiment are the 3 UAV platforms. The exit criteria for this experiment is successful navigation in confined bridge areas. The main idea of this test is to examine how easily the UAV can navigate around obstacles to carry out inspection. The UAV time constant in different channels was used as an index of its agility. The time constant, τ, is characterizing the response time to a step input.

5.13.2 Agility Test Procedure

1. Identify a suitable location that adheres to the test envelope.
2. Take-off and fly to a suitable altitude and hover the UAVs.
3. Apply a constant input (if possible maximum input) to Aileron, Elevator, Throttle, and Rudder on both directions until reaching a constant speed.
4. Log the flight data using the UAS on-board system or custom IMU-GPS system.
5. Find τ as the time when the UAS's speed reaches 0.63 of its maximum speed. In this study, the research team determined the different time constants for each of the channels and each of the directions.

5.14 Wind Gusts Tolerance Testing

The performance of UAVs (and in particular the quadrotors) is well studied in the low advance-ratio flight conditions but not well enough in largely disturbed flow conditions such as wind gusts. The real-time measurements of flow conditions around the surface of the quadrotor are required for understanding the flight condition and the influence of local wind. The key difference between wind gusts and turbulence tests are the duration and point of applied pressure. While the wind gusts tests aim to achieve impulse pressure differentials on a small area of the UAVs fuselage, the turbulence tests aim to achieve constant pressure differentials on the UAVs.

5.14.1 Wind Gusts Test Setup

The scope of this test is limited to studying the UAV platform's stability against wind gusts conditions. The test articles include the UAVs, an electric fan capable of producing wind flows ranging from 3 m/s to 5 m/s and the custom IMU-GPS flow sensor. Figure 5.8 shows the experimental setup with the UAV marked with the red box.

Figure 5.8. Setup for Wind Gust Experiment.

5.14.2 Wind Gust Test Device Development

A customized inertial and flow measurement board was constructed to capture the required measurement needed to study the behavior of the different UAVs in wind gusts. The flow measurement board consisted of a microcontroller, GPS, inertial measurement unit (IMU) and differential pressure sensors. Figure 5.9 shows the block diagram of the custom hardware. The components on the board include a microcontroller, IMU, GPS, pressure sensors and an external battery.

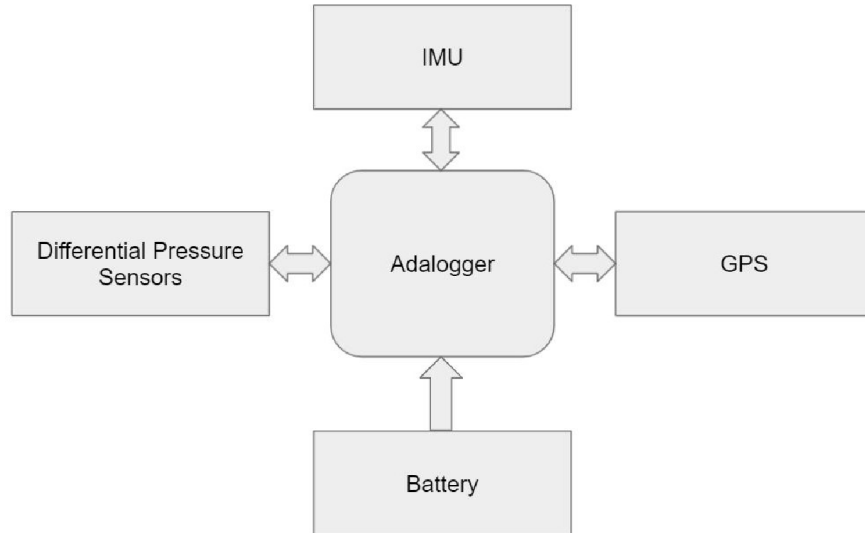Figure 5.9: Block Diagram of Custom Inertial-Flow Sensor Hardware.

Figure 5.10 shows the developed testing and measurement device which is mounted on one of the UAVs. The components of this device were carefully selected to be of small size and weight to minimize the impact on the UAV's flight dynamic.

Figure 5.10: Custom flight data collection mounted on a UAV.

5.14.3   Wind Gusts Test Procedure

1. Mount the designed pressure sensor on the top of the studied platform to measure the pressures in four directions. To reduce the effect of rotors' turbulence on the sensor measurements, sensor probes should be extended by tubes. The size and length of tubes should be chosen based on the dimension of the UAVs and its motors.
2. Apply the external disturbance using an electric fan with a varying wind speed to generate the pressure differences. The disturbances (pressure jets) will be applied horizontally which is installed on a structure with about 2m height.
3. Move the UAVs platforms on a straight line, perpendicular to the direction of the fan flow.
4. Measure the wind gust using the mounted pressure sensors.
5. The maximum acceleration experienced by the UAV as it flies and passes the fan can be obtained from the IMU logs. The impact of the wind gust on the UAVs stability is quantified in a defined metric Impact of Acceleration Change, which is computed using the following equation:

$$Impact\ on\ Acceleration\ Change = \frac{Acceleration}{DP.A}$$

Here, DP is the differential pressure that causes the maximum acceleration change and A is the surface area of the UAV the pressure is exerted.

6 TESTING AND EVALUATION RESULTS FOR THE CANDIDATE UAVS

6.1 Introduction

Using the experiments designed and described in Section 5, four commercially available UAVs having different specifications were tested to evaluate the performance of each UAV in each category. The four UAVs used are identified as UAV 1, UAV 2, UAV 3 and UAV 4 to avoid commercial advertisement. In the sections that follow, the results of each of the platform in each performance test is described, along with a comparison of how the UAVs. Special attention was paid to the implications of each UAV's performance on its potential use for bridge inspection. It is important to note that some of the platforms were not subjected to testing under some categories because the commercially available UAV did not support such functionality, or because the UAV was not available at the time of the test. In particular, UAV4 crashed fairly early in the testing program, and wasn't available for majority of the tests.

6.1.1 RF Immunity

At the onset of the RF immunity test, the test area was scanned to establish the baseline environmental RF noise in the 2 GHz frequency band. This is because each UAV tested transmits its command-and-control signal using this band. Figure 6.1 (a) depicts the control band together with the environmental noise on one of the UAVs. We observed a 5dB power level increase above the environmental noise in the bandwidth of 2.395- 2.481 GHz, when communication between the UAV and controller was established. The noise in this plot is the natural environmental noise observed prior to the introduction of artificially generated noise. Similar results were obtained for all other UAVs since they operated in the same frequency range.

6.1.2 RF Interference impacts on command signal, GPS, Video-feed

As indicated in RF immunity test description, the UAVs under test were exposed to RF interference using two methods. The first method involved the generation of a random 15 dBm continuous wave RF signal within the UAV's operating frequency range. The second method involved a 20dBm sweeping frequency within the UAV's operating frequency range. The RF noise together with environmental noises of UAV 1's control signal are shown in Figures 6.1, 6.2, and 6.3.
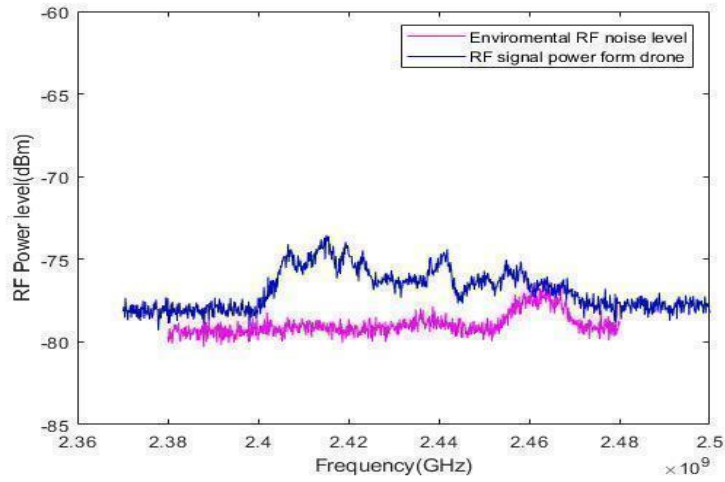
Figure 6.1 (a) : UAV control channel and environmental noise.
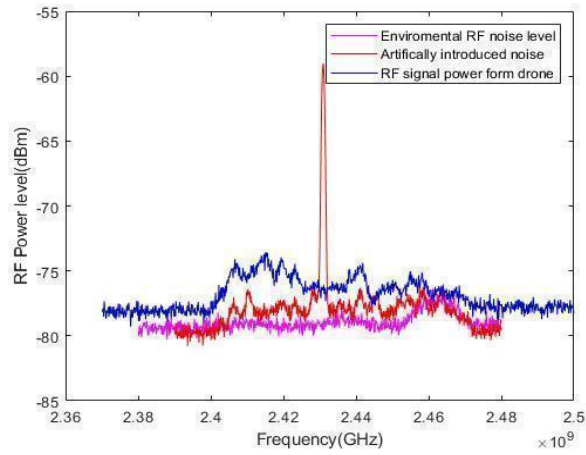
Figure 6.2 (b) : Sustained RF noise
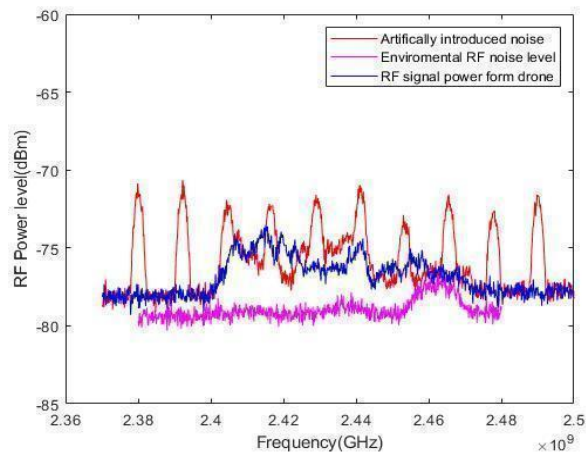
Figure 6.3 (c): Sweeping RF noise.

After the introduction of the RF noise using the two methods described above, the control commands, GPS, and video link status for UAV 1 were checked. It was observed that none of the functionalities of

44

UAV 1 were impacted for both the random 15 dBm sustained RF noise and 20 dBm sweeping noise. We repeated the above for two of the other UAVs since UAV4 had crashed and was unavailable at the time of this experiment. The results for all UAVs and test parameters using both interference generation methods are summarized in Table 6.1. and 6.1. It is evident from Table 6.1 that the connection between UAV 3 and its controller is disrupted when exposed to RF noise. The other UAVs seem to have greater RF immunity than UAV 3. The reason for the immunity differences is explained in the next section.

Furthermore, it was observed that most of the functionality of UAV 3 were impacted even at lower noise power levels than were used for the UAV 1 and UAV 2. The RF noise power above -23 dBm severely impacted the operation of UAV 3. In most cases, GPS, video, and RC signals are impacted as shown in Table 6.2. Also, when UAV 3 was subjected to a sweeping RF noise of 10 dBm in the band of its operation, we observed a reduced quality of the video feed even though the RF was working properly. This is shown in Figures 6.4 and 6.5.

Table 6.1: Sustained Noise RF immunity test results.

UAV	RF Noise	Distance to controller (m)	RC Impacts	Video Impacts	GPS Impacts
UAV 1	15 dBm power	1	None	None	None
	15 dBm power	5	None	None	None
	15 dBm power	10	None	None	None
	15 dBm power	20	None	None	None
UAV 3	15 dBm power	1	None	None	None
	15 dBm power	5	None	None	None
	15 dBm power	10	None	None	None
	15 dBm power	20	None	None	None
UAV 2	-50 dBm power	5	None	None	None
	-30 dBm power	5	None	None	None
	-17 dBm power	5	Not OK	Not OK	Not OK

Table 6.2: Sweeping Noise RF immunity test results.

UAV	RF Noise	Distance to controller (m)	RC Impacts	Video Impacts	GPS Impacts
UAV 1	15 dBm power	1	None	None	None
	15 dBm power	5	None	None	None

	15 dBm power	10	None	None	None
	15 dBm power	20	None	None	None
UAV 3	15 dBm power	1	None	None	None
	15 dBm power	5	None	None	None
	15 dBm power	10	None	None	None
	15 dBm power	20	None	None	None
UAV 2	-17 dBm power	5	None	None	None
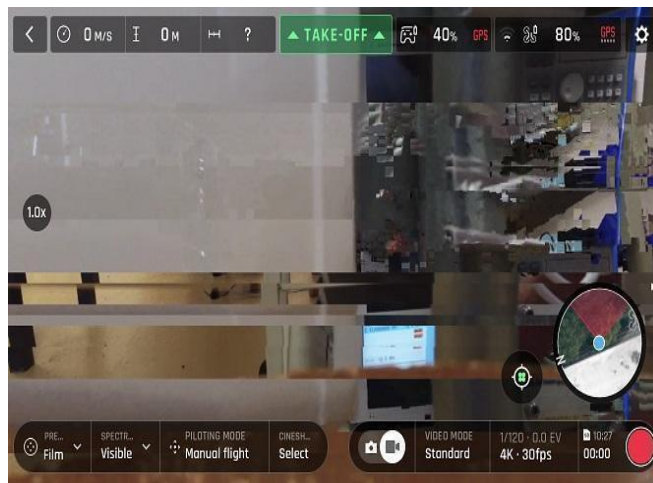
Figure 6.4: Image quality of UAV 3 for RF noise <−17dBm.

Figure 6.5: Image quality of UAV 3 for RF noise =17dBm.
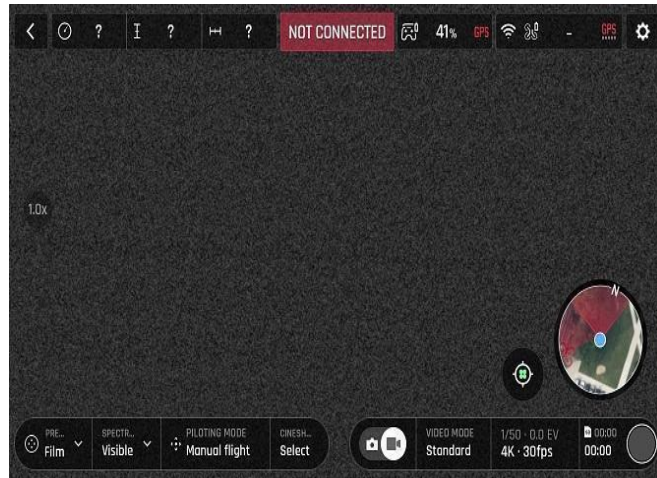
Figure 6.6: RF Channel switching between default and alternate band.

6.1.3   RF Channel switching between default and redundant channel.

It was observed that, although all UAV have inbuilt mechanism to switch to a different frequency band when the default one is impacted by a RF noise, UAV 3 takes a longer time to make the switch. In Figure 6.7, it can be observed that when an interference was introduced to the UAV 2 's default frequency (2.444 GHz), the UAV automatically switched to a different frequency, i.e., 2.461 GHz. It took the UAV approximately 15 seconds to make the switch to the new frequency and during that period all the communications were lost.
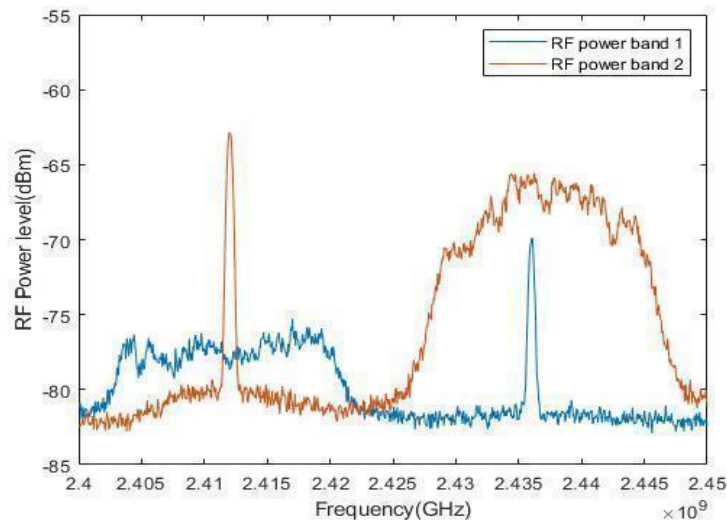
Figure 6.7: Image quality of UAV 3 after exposure to RF noise>−17dBm.

6.2 Endurance

The endurance of candidate UAVs is key to enhancing the efficiency of UAV-enabled bridge inspection. Here, the results for the endurance tests are presented for all four UAVs. The specifications document indicates the battery life of the UAV; however, this is usually measured in hovering mode. Since bridge inspection usually involves flying the UAV in the forward mode, it was imperative to test the UAV in this forward mode instead. In addition, the UAVs were also subjected to hovering mode testing to confirm the

47

endurance values indicated in the specification documents.

6.2.1   Forward mode endurance testing

Performance results in the forward mode endurance testing are very crucial to bridge inspection because this test gives an accurate depiction of the UAV's effective usage time. Unfortunately, none of the existing general-purpose UAV platforms report data on forward mode endurance in their specification manual. The endurance information provided in all the UAVs specifications manual are all based on hover mode testing. Thus, in this section, results are presented for forward mode endurance tests. In executing this test, the time it takes for the UAVs battery level to drop to 25% was measured. The time it took for the battery to reach critical levels causing the UAV to execute auto-landing for platforms that supported this feature was also determined. Additionally, the time it took for the UAV to sound an acoustic warning to the pilot to land was measured. This test was conducted outdoors and thus, an air meter was used to measure the surrounding wind speed. This was to ensure that the tests were performed in near similar conditions, enabling comparison of the results. Table 6.3. summarizes the results of forward mode endurance results for all four UAVs.

Table 6.3: Forward mode endurance test results.

UAV	Test #1	Time-to-25%-Battery Capacity (mins)	Time-to-Auto-land Warning (mins)
UAV 1	1	15	19
	2	16	20
	2	15	19
	Average	15	19
UAV 2	1	18	23
	2	20	25
	2	20	25
	Average	19	24
UAV 3	1	18	18
	2	20	20
	2	20	20
	Average	19	19
UAV 4	1	N/A	8
	2	N/A	8
	2	N/A	8
	Average	N/A	8

6.2.2 Hovering mode endurance testing

Hovering mode endurance testing was conducted indoors, in a room with all doors closed, to reduce the impact of wind. In addition, the same battery and UAV were used for all experiments. Similar to the forward mode endurance tests, the hovering mode endurance tests were divided into two parts. First, the time it took for the UAV's battery to drop to 25% of capacity was determined. This gave a measure of the UAVs effective time, i.e., the time the bridge inspections can safely be executed. Second, the time it took for the UAV to execute its auto-landing feature or sound warning to land when the battery level reaches critical levels was determined. Each of these tests was performed three times and the average was taken. Table 6.4. summarizes the results of the endurance tests.

Table 6.4: Hovering mode endurance test results.

UAV	Test #1	Time-to-25%-Battery Capacity (mins)	Time-to-Auto-land Warning (mins)
UAV 1	1	15	19
	2	16	20
	2	15	19
	Average	15	19
UAV 2	1	18	23
	2	20	25
	2	20	25
	Average	19	24
UAV 3	1	18	10
	2	20	12
	2	20	10
	Average	19	10
UAV 4	1	N/A	8
	2	N/A	8
	2	N/A	8
	Average	N/A	8

From both the forward mode and the hovering mode tests, it was observed that for UAV 3, as soon as the battery capacity reaches 25% the "land now" warning is activated. This explains the reason why the time to "Time-to-25%-Battery Capacity" and "Time-to-Auto-land Warning" are the same. For UAV 4, it was not possible to record the "Time-to-25%-Battery Capacity" because its battery management system did not provide that information. Therefore, results of only "Time-to-Auto-land Warning" were recorded. It is

evident from the results that endurance is required to perform an inspection task, UAV 2 may be the best choice.

6.3 Global Position System

The reliability and accuracy of UAV functionality relies on accurate location data provided by the GPS. One of the main challenges of UAV-enabled bridge inspection has to do with the fluctuation of the GPS signal during inspection in some more concealed locations, such as beneath the bridge deck. Therefore, when bridge inspection is carried out in locations with fluctuating GPS signals, it is vital that UAVs with reliable and robust GPS are selected. The choice of UAV should be one that has a faster "time-to-recover", when there is a disruption in the signal. Unfortunately, GPS information is not provided in the specifications document for most commercial UAVs. Therefore, the motivation for this test was to serve as a guide selecting UAV for GPS-critical inspection.

6.3.1   GPS time-to-recover

This test was performed in stationary mode where the UAV is not flying. For UAV 2 and UAV 3, it was possible to obtain the GPS information while the UAV was stationary. UAV 1 was not tested because its GPS information is only available in-flight mode. UAV 4 does not have GPS support. This may seem to be a disadvantage. However, this can prove to be an advantage when the UAV is in consideration for inspection in a GPS-denied environment. Table 6.5. summarizes the results for the GPS for UAV 1 and UAV 3. The results indicated the GPS recovery time for UAV 3 is superior as compared to UAV 2.

Table 6.5: GPS time to recover.

Time-to-recover (seconds)											
UAV / Test #	**1**	**2**	**3**	**4**	**5**	**6**	**7**	**8**	**9**	**10**	**Average**
UAV 1	9.98	9.81	8.59	10.71	9.41	8.53	8.56	7.96	9.15	9.96	9.26
UAV 2	N/A	N/A	N/A	N/A	N/A	N/A	N/A	N/A	N/A	N/A	N/A
UAV 3	7.93	6.53	5.77	5.98	6.98	7.24	6.26	5.92	5.81	7.93	6.58
UAV 4	N/A	N/A	N/A	N/A	N/A	N/A	N/A	N/A	N/A	N/A	N/A

6.4 Autonomy

In this section, we present the results of the three autonomy tests namely, auto-land, waypoint following, and return-to-home. From these tests it was observed that only UAV 3 supported all the autonomous functionality. UAV 1 and UAV 2 supported auto-land and waypoint following, but not return-to-home functionality. UAV 4 supports none of the autonomous functionality. Table 6.6. summarizes the results of the test.

Table 6.6: Autonomy test results

Platform	Auto-Land	Waypoint following	Return-to-Home
UAV 1	Yes	Yes	No
UAV 2	Yes	Yes	No
UAV 3	Yes	Yes	Yes
UAV 4	No	No	No

6.4.1   Illumination

Results of the illumination experiment were obtained for only three UAVs, because at the time of the experiment, the UAV 4 had crashed. Each row of Figure 6.8 shows how the UAVs' camera performs in similar light conditions. As explained before, level 4 indicates that lightning level is maximum, and level 1 indicates minimum lightning. It is evident from the results that the ability to detect the defects in the test element decreases with visibility. The results show that UAV 3 has superior camera performance as compared to UAV 1 and UAV 2. Also, we studied the proximity of the UAVs to the test element under different lighting conditions affects the ability to detect defects in the test element. It was observed that the camera performed poorly when larger distances existed between the UAV and test element. This made detecting defects impossible in the low visibility scenarios. The results highlight the need to fly as close as possible to an element under inspection.

(a) UAV 1   *(b)* UAV 2   *(c)* UAV 3

Figure 6.8(a): Illumination level 4 (> 250 lx)

(a) UAV 1   *(b)* UAV 2   *(c)* UAV 3

Figure6.8. (b): Illumination level 3 (220 – 250 lx)

(a) UAV 1   (b) UAV 2   (c) UAV 3

Figure 6.8.(c). Illumination level 2 (120-220 lx)

(a) UAV 1   (b) UAV 2   (c) UAV 3
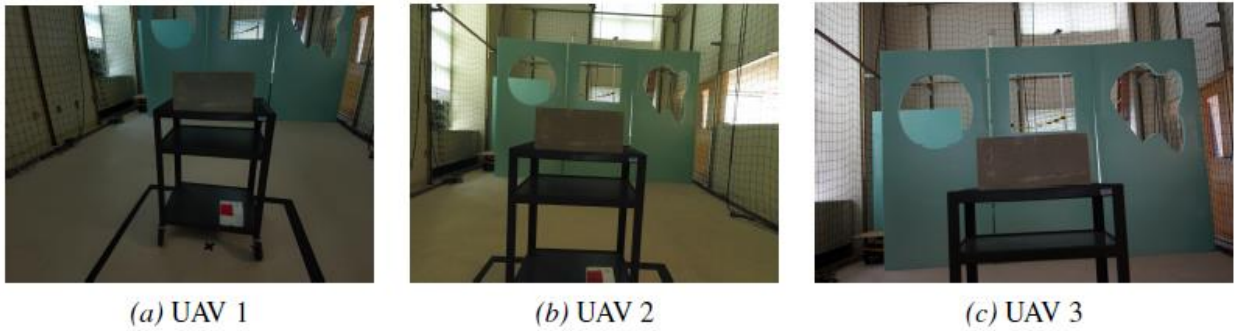
Figure 6.8. (d). Illumination level 1 (10-130 lx)

The entropy of the images captured for the various images at the different illumination levels was also computed. The observations were made by visually inspecting the images' match with the entropy calculations. UAV 3 had a higher entropy across all levels as compared to the entropy of UAV 1 and UAV 2.

The entropy of the images captured at the different illumination levels was also computed, with the match between each image and the entropy calculations observed. UAV 3 had a higher entropy across all levels as compared to the entropy of UAV 1 and UAV 2.

To corroborate the results obtained from the lab environment with field conditions, the team attempted to replicate a similar experiment in an actual bridge environment. Since the illumination level at the bridge site could not be controlled, one column of the bridge with different illumination conditions at each of the four sides was selected. It is worthy of note that the field experiment was impacted by the prevailing wind gusts, thus the images captured, although similar, may have slight wind-induced variations. Furthermore, this field experiment was conducted using only two UAVs (UAV 1 and UAV 2) because operating UAV 3 in the presence of wind gusts in GPS-denied environments was determined to be too challenging. Although it was impossible to measure the illumination level at the four faces of the column, based on visual inspection, the illumination levels were labeled Level 1, Level 2, Level 3 and Level 4. Similar to the lab tests, level 1 corresponds to the lowest illumination condition, with level 2 and level 3 being intermediate levels and level being the highest illumination level. The results of the field experiment are shown in Figure 34. Similarly, it is evident by visual inspection that UAV 2 performed better than UAV 1, which corroborated the result from the lab environment.

(a) UAV 1   (b) UAV 2

Figure 6.9: Illumination Level 4

(a) UAV 1   (b) UAV 2

Figure 6.10: Illumination Level 3

(a) UAV 1   (b) UAV 2

Figure 6.11: Illumination Level 2

(a) UAV 1   (b) UAV 2

Figure 6.12: Illumination Level 1

The entropy of each of the images acquired by UAV 1 and UAV 2 was computed under the different illumination levels. Here also, the results are consistent with the lab environment results. It is observed from Table 13, in all the cases, the entropy of the images captured with UAV 2 is higher than that of UAV 1.

Table 6.7: Entropy of Images for Each UAV (Bridge Site)

Platform	Level 1 (Dark)	Level 2	Level 3	Level 4 (Bright)
UAV1	6.96	6.95	7.41	7.61
UAV2	7.38	7.40	7.53	7.58

6.4.2   Vibration

The vibration test was executed with UAV 1 and UAV 2. This experiment could not be performed with all

of the candidate UAVs because UAV 3 had difficulties taking successive images with an interval of about 1 second. Also, UAV 4 was not available at the time of the experiment due to the aforementioned crash. As described in the experiment section, two images were captured at intervals of about 1 second, and this process was repeated 14 times. For each of the 14 two-second interval images, the first image was considered as the reference and the peak-signal-to-noise-ratio (PSNR) between the reference images and the second image was computed. Table 6.7 shows the noise that was introduced as a result of the vibration for UAV 1 and UAV 2. It is observed that the PSNR of UAV 2 is, on average, lower than the PSNR of UAV 1. It thus indicates the gimbal of UAV 2 is more stable in the presence of vibration than that of UAV 1.

Table 6.8: Vibration impact on PSNR

Platform															Average
UAV 1	16.59	16.92	16.42	15.79	19.21	22.74	20.70	19.90	22.14	22.74	22.79	21.06	21.14	21.04	19.95
UAV 2	16.47	17.37	19.46	13.85	17.96	21.85	14.09	19.83	19.11	20.43	19.95	19.62	17.99	13.89	17.99
UAV 3	N/A	N/A	N/A	N/A	N/A	N/A	N/A	N/A	N/A	N/A	N/A	N/A	N/A	N/A	N/A
UAV 4	N/A	N/A	N/A	N/A	N/A	N/A	N/A	N/A	N/A	N/A	N/A	N/A	N/A	N/A	N/A

6.5 Wind Gusts Tolerance

From this experiment, it was observed that whenever the UAV flies in a direction perpendicular to the wind, a force is exerted on it which causes it to deflect away from the source of wind gust. This deflection which is equivalent to the force exerted on the UAV is calculated by identifying the maximum UAV acceleration from the IMU logs. The impact of the wind gust on the UAV is computed using Equation 4.4. Table 15 shows the acceleration changes due to the wind gusts on UAV 1 and UAV 2. From the results, it is evident that UAV 2 experiences the greatest impact when it flies past the fan. These results are consistent with the observation of the pilot, who indicated he had to provide additional force to counteract the effect of the wind gust for UAV 2 as compared to UAV 1 in the pressure of the wind gust.

Table 6.9:Wind Gust Impact on Acceleration Change

Platform	Impact on Acceleration Change
UAV1	1090.40
UAV2	17049.41

6.6 Reassessing the selection of the UAVs

We started with selection, test, and evaluation of four UAVs among which UAV3 was found very vulnerable in the presence of wind gusts in GPS-denied environments and UAV4 crashed early in the testing program and wasn't available for majority of the tests. Looking back in Table 3.11, we can also observe that the AHP process would suggest that UAV 1 and UAV 2 with higher scores, are more appropriate choices for bridge inspection. Note that the AHP process was conducted to select UAVs even before conducting the test and evaluation experiments, primarily based on the available information in catalogs, technical manuals, and other available resources about the UAVs. In our particular case-study, most experimental results confirmed the superiority of UAV 1 and UAV2, which is consistent with the AHP results summarized in Table 3.11, and hence, we do not need to revise the AHP weights. Excluding UAVs 3 and 4, the AHP-based scores of UAVs 1 and 2 are shown in Table 6.10 which are relatively similar.

Table 6.10: Scores of UAVs 1 and 2

	UAV 1	UAV 2	Criterion Weight
Can look upward	0.0504	0.0504	0.2015
Gusts Tolerance	0.0272	0.0272	0.0926
Autonomous	0.0251	0.0251	0.0801
Gyro	0.0146	0.0146	0.0584
Ultrasonic	0.0302	0.0060	0.0483
Accelerometer	0.0117	0.0117	0.0466
Wind Tolerance	0.0108	0.0108	0.0397
Endurance	0.0114	0.0191	0.0381
Defualt Payload	0.0116	0.0087	0.0376
All-weather ability	0.0078	0.0078	0.0311
Custom payload?	0.0068	0.0068	0.0273
Max Payload weight	0.0052	0.0052	0.0207
NavCam	0.0051	0.0051	0.0205
Net Weight	0.0050	0.0050	0.0198
Number of Engines	0.0047	0.0047	0.0187
GNSS	0.0042	0.0042	0.0169
Compass	0.0038	0.0038	0.0152

Environmental Temperature Range	0.0019	0.0019	0.0148
Communication Link Range	0.0028	0.0028	0.0140
RC Range	0.0028	0.0028	0.0140
Magnetometer	0.0027	0.0027	0.0107
Max Airspeed	0.0019	0.0019	0.0074
Max Climb Rate	0.0013	0.0013	0.0066
Max Alt.	0.0016	0.0016	0.0062
Live stream	0.0015	0.0015	0.0058
Beyond Line-Of-Sight Range	0.0014	0.0014	0.0056
Frequencies	0.0012	0.0012	0.0048
Low latency	0.0008	0.0008	0.0032
Encryption0.0003	0.0003	0.0003	0.0012
Final Score	0.2743	0.2549	1

Note that the pair-wise comparison weights in the AHP process are subjective numbers, reflecting the opinion of the experts/testers. Hence, if after conducting test and evaluation experiments one decides to reassess the proposed AHP-based selection framework by revising the pair-wise comparison weights, only Table 3.10 needs to be revised to update Table 3.11, assuming that the weights of selection criteria remain unchanged.

7 FIELD TRIALS

7.1 Test flights at Structure 620072

Structure 620072 in Moore County, NC was selected as an in-service bridge for test flights. This structure was constructed in 1967. It crosses a water feature but has several spans over the land. This structure has been used for a UAV demonstration previously, but only for flights beside and underneath the bridge. Previous flights were not carried out above the bridge deck. A photo of this structure is shown in Figure 7.1. This structure has been in service for several years, and currently exhibits significant distress, particularly in the concrete pier caps, concrete columns, some retrofit steel members, and the concrete deck.

Figure 7.1: Overview of structure 620072 in Moore County.

Several tests were conducted in April and May 2021 to test the platforms including test of resilience to loss of GPS, quality of images and data collection. Prior to the flights, the inspection reports for this bridge were reviewed. The most recent inspection report for structure 620072 (April 22, 2020) was obtained from NCDOT's Structures Management Unit. Using the inspection report as a guide, a punch list of elements was identified prior to the test flights. These included locations identified as Priority Action Requests on the inspection report, as well as other locations where distresses were documented. Effort was made to select locations that included distresses of different severity levels, as well as distresses on different types of elements. After performing the flights, the video was reviewed, and a separate video containing highlights of the test flights was prepared.

Below, several still photographs captured from the video obtained by the UAV are shown. As can be observed, the UAV effectively gathered images of the quality typically shown in many inspection reports. Additional descriptions of the bridge elements, distress types, and site conditions are provided in the captions beneath each photograph.

Figure 7.2 Debris pile from high flow event piled against column. Using imaging analysis technology, the volume of the pile could likely be calculated to assist in debris removal activities.

Figure 7.3: Debris pile from high flow event piled against column. Using imaging analysis technology, the volume of the pile could likely be calculated to assist in debris removal activities

Figure 7.4 Spalls on column, corroded longitudinal steel. At closer magnifications of the image, the deformations on reinforcing bars are visible, as well as cracks alongside the spalled areas. Note the condition of the channel bottom is also evident.
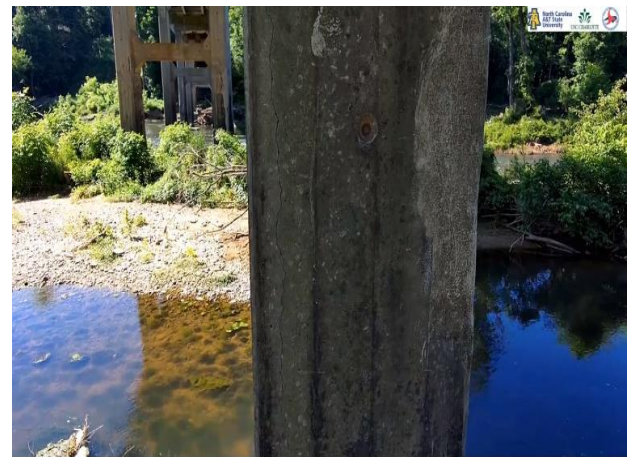
Figure 7.5: Cracks on pier over longitudinal steel. Staining evident, indicating initiation of corrosion.

Figure 7.6 Hairline cracks visible on underside of concrete deck.

Figure 7.7: Crack on underside of pier cap, following longitudinal steel. Discoloration and staining evident from drainage.

Figure 7.8: Diaphragm with bolted and welded connections shown, along with condition of concrete pier cap. Condition of bearing pad, plate, and bolts can also be observed.

Figure 7.9: Steel plates bolted onto pier cap, with corrosion evident. Condition of girder, diaphragms and connections can also be observed.

Figure 7.10: Spall with exposed, corroded rebar in concrete diaphragm overhang. Condition of drainage pipes and utility conduit can also be observed.

Figure 7.11: Staining on underside of girders.

Figure 7.12: Staining and cracking in pier cap. Condition of girders and diaphragm is also evident.

Preliminary flight tests at structure 620072 were largely successful. Two different candidate UAVs demonstrated adequate performance at a field structure in typical (to favorable) weather conditions. The research team gained valuable insight into the necessary planning required to begin integrating these two UAVs into the inspection workflow. Experience was gained regarding the flight plan, such as the number of flights required to inspect a structure of this size/configuration/condition, the quantity of bridge elements/area of bridge that could be reasonably inspected on each battery, amount of time lost to UAV setup and non-inspection travel. Additional insight was also gained into the quality of images that could be obtained in different illumination conditions, geometric configurations, and camera angles. From an inspector's standpoint, images captured by the UAV could be directly compared to those obtained during the conventional inspection, providing confidence in their quality. Although not quantified or qualitatively assessed, the distresses visible in the UAV-obtained video and images could be assessed per the inspection protocol and compared to the ratings and quantities provided in the latest inspection report. It is noted, however, that there was a time lag of over a year between the conventional inspection and these UAV field trials. In conclusion, field trials at structure 620072 provided valuable insight into the work needed to integrate the candidate UAV platforms into the inspection workflow, which will be phase 2 of this work.

8 IMPLEMENTATION AND TECHNOLOGY TRANSFER PLAN

Research Product 1	AHP UAV selection procedure
Suggested User	NCDOT Division of Aviation and Structures Management Unit
Recommended Use	The Analytic Hierarchy Process (AHP) methodology can be adopted for the multiple-criteria decision making (MCDM) and comparing the capabilities of multiple UAS platforms. The AHP methodology can be applied to different criteria (in this case, 32 criteria) defined under major categories including flight performance, situational awareness, payload and sensor capabilities, and communication quality. The procedure requires a pairwise comparison in a hierarchical manner at the category level, criterion level, and candidate platform level. The results from comparisons are integrated to an AHP table and can result in the selection of the most suitable UAS for bridge inspection in the defined scenario. This should help NCDOT to systematically select UAS for bridge inspection purposes based on the priorities and desired performances.
Recommended Training	None at this time.

Research Product 2	Methods of test and evaluation of UAVs for bridge inspection
Suggested User	NCDOT Division of Aviation and Structures Management Unit
Recommended Use	The designed experiments can be used to test and evaluate the UAVs for bridge inspection as an effort for certification of UAVs for the agent-wise adoption of UAVs. This should help NCDOT to develop a certification procedure for adopting UAS for bridge inspection purposes.
Recommended Training	None at this time.

Research Product 3	Weather Data Collected at the Bridge on US 70 Eastbound (structure 4) over the East End Connector in Durham, NC
Suggested User	NCDOT Division of Aviation and Structures Management Unit
Recommended Use	Temperature and wind data over multiple periods of time and measurements at multiple locations of the bridge structure were archived for future use.

Recommended Training	None at this time
Research Product 4	Initial Inspection Data Collected by UAVs at Selected Structures
Suggested User	NCDOT Structures Management Unit
Recommended Use	Review to inform progress on phase 2 of this work, aimed at integrating UAVs into bridge inspection workflows and using UAV-acquired data to support completion of bridge inspection reports.
Recommended Training	None at this time.

9 CONCLUSION

As part of this project, a hierarchical MCDM framework development for UAS-enable bridge inspection selection practices was introduced. The framework employed a hierarchical method to analyze 32 criteria categorized in Flight Performance, Situational Awareness, Payload and Sensor Capabilities, and Communication Quality. Using the AHP methodology, the significance of each criterion with respect to the bridge inspection was numerically quantified through pairwise comparisons. Furthermore, the AHP methodology was implemented to quantitatively compare each of the candidate UAS platforms' performance with respect to each criterion. The result of this methodology implementation on the candidate platforms obtained a fair and comprehensive comparison of their suitability with respect to each criterion. By incorporating available UAS platforms and user preferences and then scoring their overall capabilities, the framework will allow the decision makers to select the most suitable UAS for different bridge inspection practices. This initial UAS-enabled bridge inspection decision making framework can be applied to other situations, as long as the pairwise comparisons meet the AHP consistency constraint.

The weather data gathered by the mounted weather station provided valuable information for the computational modeling and the design of experiments for the UAV flights. For this work only the temperature information was not utilized but was archived for future researchers. The gathered wind data included direction, average speed, and gust speed. The wind conditions at deck level provided boundary conditions for the computational models. The wind conditions gathered at both locations under the bridge confirmed the significant shielding the structure provides. The data also supported the simulation findings that the forces encountered by the UAV under the bridge results from the specific geometry of the bridge components. The computational modeling of the bridge sections showed the increased velocity and turbulent energy is found as the air flow is directed through the diaphragms resulting in jet-like behavior. Simultaneously, low force areas are found near the gusset plate and concrete bends where shielding occurs. These large variations in air flow and resulting forces are important to the flying of the UAV.

Further, the advantages offered by UAVs when used as a tool for bridge inspection were explored. Four feature categories and their sub features that should be taken into consideration when selecting UAVs for bridge inspection were identified and discussed. In addition, simple experiments for testing and evaluation of various capabilities of UAVs by subjecting the UAVs to the various testing conditions were developed and presented. This enabled the comparison of different commercially available UAV platforms based on the needs of an inspection mission. Results indicated that the candidate UAVs have different performance characteristics. Therefore, testing and evaluation is crucial in identifying UAVs that will perform effectively under different bridge inspection scenarios. The tests developed as part of this work and described herein could be modified and utilized in the future to evaluate new UAVs that may become available as this area of product development is rapidly growing and advancing. Overall, out of four UAVs which were gone through the developed T&E experiments, UAVs 1 and 2 were found more effective solutions for bridge inspection particularly due to their ability to fly underneath of the bridge. This was confirmed both by an AHP process conducted before the experiments for selecting the UAVs and through the experimental results in a consistent way.

Preliminary flight tests at a 10-span bridge exhibiting significant distress were largely successful. Two different candidate UAVs demonstrated adequate performance at a field structure in typical (to favorable) weather conditions. The research team gained valuable insight into the necessary planning required to begin integrating these two UAVs into the inspection workflow. Experience was gained regarding development of the flight plan and the logistics of inspection of a structure of this size/condition using the candidate UAVs. The images captured by the UAV could be directly compared to those obtained during the conventional inspection, providing confidence in their quality. Distresses visible in the UAV-obtained video and images could be compared to the ratings and quantities provided in the latest inspection report, again providing confidence in the ability of the UAVs to gather specific data required to be included on a

bridge inspection report. Overall, field trials at structure 620072 provided valuable insight into the work needed to integrate the candidate UAV platforms into the inspection workflow, which will be phase 2 of this work.

Future Research Needs

Future research needs based on the outcomes of this project includes different dimensions as briefly listed below:

- UAV and payload setup:
  a. A set of checklists for calibration and set up the sensors and UAVs for bridge inspection.
  b. Sensor fusion for detecting problem spots and their severity at different bridge elements.
- Data archiving and processing:
  c. A procedure for archiving huge data being collected during the UAV-assisted inspection.
  d. Data-analytic tools for initial assessment of UAV-assisted data.
- Bridge and near-bridge analysis
  e. A systematic study of bridge element sizes and configurations in combination with a more extensive variation of weather conditions. This study would support the development of a guide that would provide fly/no-fly guidelines based on a set of critical bridge information. This guide would allow the inspector and/or UAV pilot to obtain bridge specific information without the length process of model create and CFD analysis.
- Workflow development for adopting UAVs for bridge inspection:
  f. Guidance regarding identification of candidate bridges for UAV-assisted inspection (e.g. characteristics of bridges that make them good candidates for use of a UAV to supplement inspection vs. characteristics of bridges that make a structure less desirable for use of a UAV to supplement inspection.
  g. Guidance to support integration of data collected by UAV into inspection reports. A workflow (or workflows) to support UAV-assisted inspection, including logistics and considerations required for pre-inspection, during inspection, and post-inspection.

APPENDICES

FOR
FINAL REPORT

North Carolina Department of Transportation
Research Project No. 2020-23

UAV Selection Methodology and Performance Evaluation
to Support UAV-Enabled Bridge Inspection

By

Ali Karimoddini, Ph.D.
Associate Professor

Tara L. Cavalline, Ph.D., P.E.
Associate Professor

Beth Smith, Ph.D.
Assistant Professor

Rodward Hewlin
Assistant Professor

Abdollah Homaifar
Professor

Edward Mahama
Graduate Research Assistant

North Carolina Agriculture and Technical State University
1601 East Market Street Greensboro, NC, 27411

March 2022

A.1 APPENDIX A – EXTENDED LITERATURE SURVEY ON TESTING AND EVALUATION OF UAV-ENABLED BRIDGE INSPECTION

A.1.1 Introduction

Regular inspection is imperative to maintain the bridges for road safety and to lengthen the lifespan of bridges. Like many states, NCDOT and their contracted partners perform thousands of inspections annually. Due to resource reductions, time limitations, increased traffic, restrictions on lane closures, and other factors, there is the need for exploring the use of modern technology and equipment that can help to improve the efficiency of the existing methods and mitigate the risks associated with the traditional bridge inspection methods. Here, a discussion on the existing bridge inspection techniques and their challenges is presented. It also introduces UAV-enabled bridge inspection and discusses its pros and cons. Finally, previous contributions to UAV-enabled bridge inspection are also discussed in depth.

A.1.2 Conventional Bridge Inspection Techniques

Existing bridge inspection techniques are demanding, less efficient and can sometimes expose inspection personnel to danger. They usually require special equipment such as cranes, snooper trucks, scaffolds and rope access. Figures A-1, A-2 and A-3 show the equipment in action for bridge inspection. Inspection of the under-deck of bridges, requires snooper trucks to be stationed on the bridge deck. This means that a lane will have to be closed for inspection, impacting free flow of traffic and causing inconvenience to road users.

In addition, there are certain bridge components that are difficult to reach and therefore require rope access for inspection. This can expose the lives of inspection personnel to danger. Also, specially trained professionals such as industrial climbers are employed to access special parts of the bridge, but they usually have little to no knowledge of component damages detected. Thus, they can only take photos and videos of identified defects to be analyzed later by civil engineers. Thus, real-time inspection of components is most often not possible.

Furthermore, in the traditional inspection techniques, defects detected are documented manually in reports. Inspection personnel typically use textual descriptions and photos to document observed defects. The outcome of these recorded defects relies heavily on the experience of inspection personnel and can also be easily affected by the mood of the inspectors.

In view of the challenges with the traditional inspection techniques, there has been a conscious effort to find alternative inspection means or tools that can supplement the existing methods. UAVs seem to be a viable tool that can mitigate most of these challenges. As such, several departments of the transportation (DOTs) across the United States have been exploring UAVs feasibility for bridge inspection. In the next section, potential benefits of UAVs for bridge inspection are discussed.

Figure A.1: Figure A-1. Scaffolds [78].

Figure A.2: Snooper trucks [79].

Figure A.3: Rope access [80].

A.1.3 UAS-Enabled Bridge Inspection

UAVs are small aircraft that can be flown remotely either in autonomous mode or in manual mode by a pilot with the help of a controller. Traditionally, they were used solely by the military for Traditionally, they were used solely by the military for combat and reconnaissance missions. However, in recent times they are receiving an increasing level of attention for their use in a variety of civil applications such as, remote sensing [81], search and rescue missions [82], disaster management [83], courier services [84], security and surveillance [85], wireless coverage [86], precision agriculture [87], and infrastructure inspection [88].

The main drivers for the popularity of UAVs in civil applications are advances in UAV technologies, driving the cost of UAVs down. Furthermore, in the last decade, there have been tremendous advances in remote sensing technologies such as light detection and ranging (LiDAR) and photogrammetry. The combination of these two drivers have thus made UAVs attractive in many civil applications. In fact, bridge inspections seem to be the one application area that is receiving attention due to cost and safety advantages they offer. Several DOTS in the United States have been exploring the use of UAVs for bridge inspection. Figure A-4 shows states that have in the past explored the use of UAVs for bridge inspection or is currently investigating its use.
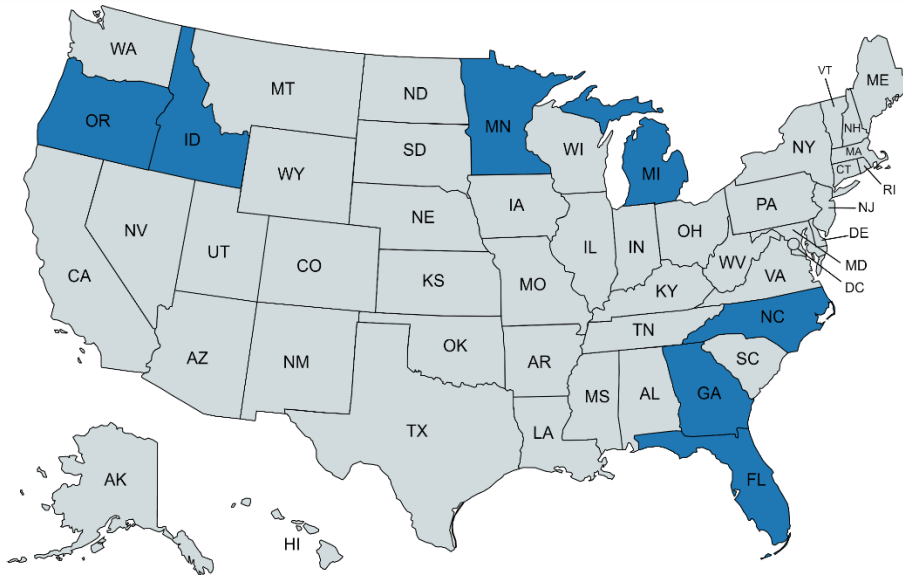
Figure A.4: State DOTs with current or past UASs exploration.

A.1.4 Benefits of UAS-enabled bridge inspection

The benefits that come with the use of UAV for bridge inspections are both technical and economic. They eliminate the risk associated with the traditional bridge inspection methods such as rope access discussed above. UAVs can be remotely piloted to inspect bridge components that will otherwise require roped access and putting the lives of inspection personnel at risk [17]. In fact, safety advantages afforded using UAVs were reported by experimenting with UAV-assisted bridge inspection by some DOTs [60, 76, 89]. In addition, UAS-enabled bridge inspections are economical since no specialized equipment such as snooper

trucks, scaffold, ladders, etc. are required for inspection [90]. Thus, data can be acquired without the need for this specialized equipment resulting in reduced bridge inspection cost. Also, UAVs can also offer real-time bridge inspection. It is possible to mirror the screen of the pilot onto another screen which can be viewed by inspectors. The inspectors can thus take a snapshot of identified defects for further examination later. Furthermore, it takes less time to execute an inspection task as compared to the traditional inspection techniques [90]. With UAVs the use of specialized equipment is eliminated except in special instances where UAVs cannot suffice. In scenarios where it is too difficult to reach bridge components, UAV take less time as compared to roped access or snooper trucks [17]. Finally, all the remote sensing technologies for bridge inspections are non-contact techniques that leads to minimal traffic disruption and require low labor [88]. The collected data is a soft-copy and thus it makes the easy application of advanced data analysis techniques.

A.1.5 Challenges of UAS-enabled bridge inspection

The main hurdle that restricts the use of UAVs for bridge inspection is government regulations. Current Federal Aviation Authority (FAA) regulation for instance, allows UAVs to be used for bridge inspection only if there is no traffic in sight [90]. Therefore, for bridge deck inspection, the road still needs to be closed although no access equipment will be needed. There is also the restriction of beyond-line-of-sight flight [33]. The pilot of the UAV is required to always have visual contact with the UAV during inspection even if the UAV has live streaming capability.

Another challenge is the UAV capability limitations [90]. This can range from the ability to operate in a GPS-denied environment [90], bad weather [17] and the flight time [33] of the UAV. The small size of the UAVs makes them susceptible to wind gusts rendering them difficult to control during inspection [17]. Also, under deck inspection usually must be executed in manual mode since there is usually limited or no signal under the bridges. In addition, most UAVs cannot fly continuously for more than 1 hour. This means that inspection must be stopped intermittently for the battery to be replaced which can sometimes be inconvenient for large bridges. In addition, some bridge inspection tasks requiring physical contact, such as determining the width of cracks, cleaning bridge elements to remove rust or dust for detailed defect observation cannot be accomplished with UAVs [17]. Therefore, in those instances traditional methods will have to be relied on. Furthermore, there is no one fit all UAV that can perform a complete bridge inspection. For instance, a UAV equipped with an ultrasonic sensor may be suitable for bridge deck inspection, however, components such as bearings that require close examination can be a challenge. This is because ultrasonic sensors restrict the minimum clearance between the UAV and bridge. Thus, in such scenarios it is required to choose a UAV that can get as close as possible to the bridge. Finally, there is no available comprehensive guide on testing the various UAV criteria for a specific task. This is particularly important for inspectors to have a fair idea of how the chosen UAVs will perform when use for inspection.

A.1.6 Related works

There are several studies that have investigated the use of UAVs for bridge inspection. The forerunners of most of these studies are the state DOTs usually in partnership with academia.

In [33], UAV-enabled bridge inspection methodology is investigated. This led to the development of a five-stage bridge inspection workflow which are bridge information review, site risk assessment, pre-flight

setup, UAVs-enabled inspection and data processing. The UAVs used were chosen based on flight time, upward viewing camera capability, camera resolution, video resolution, payload capacity, illumination and communication range. Although the criteria are crucial for bridge inspection, they are limited. There are some criteria that can greatly impact the effectiveness of the UAV for bridge inspection that was not included. For instance, the results of [91], showed that fluctuation in wind speed caused by atmospheric turbulence and body generated turbulence can impact the quality of images captured during inspection. In addition, in [92], we showed that the presence of electromagnetic interference can impact the effectiveness of UAVs for bridge inspection. There are other crucial criteria such as live-stream capability, autonomy, maneuverability etc. which were not taken into consideration in selecting the UAVs bridge inspection. Furthermore, the selection of the UAVs was based mainly on the specification document provided by the UAV manufacturers. This restricts the criterion upon which the UAVs can be assessed since some of the important criteria such as interference immunity is usually not specified in the specification's material.

In [89], Minnesota DOT in collaboration with Collins Engineering reported their findings on the challenges and benefits of UAVs for bridge inspection. This work was carried out using four different bridges in order to evaluate the effectiveness of the UAVs for inspecting different types of bridges. The selected bridges used in the study are long single span prestressed concrete bridge, open spandrel concrete arch bridge, a five-span steel underdeck truss and five truss arch spans. Some of the challenges mentioned in this work are the inability to use chosen UAVs to inspect the under deck of bridges and the inability of some of the UAVs to operate in GPS denied environments. They also reported scenarios where UAVs were able to detect defects that were missed by the traditional inspection techniques. Also, they indicated the restriction imposed by FAA rule that prevents the inspection of bridges with traffic. They however reported that safety and cost advantages far outweigh the challenges they encountered.

The Michigan Department of Transportation reported their results of the exploration of 5 different UAVs for bridge inspection [60]. This work was conducted using a combination of payload sensors including visual cameras, infrared cameras, and LiDAR sensors. They reported effectiveness of a particular UAV depends on the bridge inspection scenarios. For instance, they reported that a UAV equipped with thermal sensors was the most effective tool for delamination detection in bridge deck. In a nutshell, this work recommended UAV use for inspection as they are cost and time effective tools for bridge inspection.

Florida DOT of transportation also investigated the feasibility of using UAVs as a supplementary tool to traditional bridge inspection methods [89]. They indicated in their report that a UAV-assisted inspection can lead to an improved cost of inspection, minimized inspector exposure to danger, increased public safety, and facilitated effective data acquisition and storage. Also, they identified payload weight limitation, stability of control system in wind gusty situations and deterioration of image quality in bridge areas with limited illumination as the main challenges. One aspect of this work was the development of a systematic decision-making toolbox for the selection of UAVs depending on the inspection requirements. Furthermore, they also estimated the minimum clearance the selected UAV can safely operate in prevailing wind gusts between 11km/h to 16 km/h.

The authors of [93] proposed some basic guidelines regarding the use of Remotely Piloted Aircraft Systems (RPAS) for surveys and inspection. One component of the proposal involved the technical considerations and characteristics of the device for inspection. The technical consideration was mainly on ultrasonic and camera capabilities of the UAV. While these two criteria are crucial for inspection, it is not

adequate to decide on which UAS to be selected for bridge inspection. A UAV can be equipped with a good camera but without a good control system to tolerate turbulence around bridges, it may be ineffective for bridge inspection. There are other criteria highlighted in previous discussion essential for UAS-enabled inspection that need to be tested and evaluated.

The development and characterization of experimental testing of a multi-rotor UAS in wind tunnel is presented in [94]. The setup was used to simulate the adverse wind conditions that UAVs are most likely to encounter in bridge inspection conditions. This relied on portable fans for generating indoor wind disturbances in order to examine the UAVs response to wind turbulence. The frequency content of the wind generated during the experiment is analyzed to identify suitable excitation for UAV. The result of this served as a guideline for testing and selecting UAS likely to be used in wind turbulent conditions. This work focused on testing just one criterion.

The previous studies that explored UAVs for bridge inspection placed less emphasis on the UAV selection. Also, previous research that performed testing and evaluation of UAV capability have a comprehensive treatment of usually one feature. With regards to the selection, the authors relied on very few parameters. In most cases no test was conducted by the authors to verify if the UAV can withstand bridge conditions. As a result of the sole reliance on information in the specification documents, important criteria such as RF immunity and GPS robustness is rarely taken into consideration during UAV selection. Therefore, in this work, we pursue a holistic approach by first identifying a comprehensive list of important UAV criteria for bridge inspection. We go a step further by coming up with simple experiments to test these features. We use a combination of qualitative and quantitative means wherever appropriate to report our results.

A.2 REFERENCES

[1] 2021, Infrastructure report card. Available: https://infrastructurereportcard.org/wp-content/uploads/2020/12/Bridges-2021.pdf

[2] P. C. Tung, Y. R. Hwang, and M. C. Wu, "The development of a mobile manipulator imaging system for bridge crack inspection, "Automation in construction, vol. 11, no. 6, pp.717–729, 2002.

[3] J.-K. Oh, G. Jang, S. Oh, J. H. Lee, B.-J. Yi, Y. S. Moon, J. S. Lee, and Y. Choi, "Bridge inspection robot system with machine vision, "Automation in Construction, vol. 18, no. 7, pp. 929 – 941, 2009.

[4] B. Sutter, A. Lelev́e, M. T. Pham, O. Gouin, N. Jupille, M. Kuhn, P. Luĺe, P. Michaud, and P. R emy, "A semi-autonomous mobile robot for bridge inspection, "Automation in Construction, vol. 91, pp. 111 – 119, 2018.

[5] Irizarry, J.a.J., E.N., "Feasibility Study to Determine the Economic and Operational Benefits of Utilizing Unmanned Aerial Vehicles (UAVs)". Final Report, Georgia DOT Research Project 12-38. Georgia Department of Transportation, 2014.

[6] Dorsey, T., "35 State DOTs are Deploying Drones to Save Lives, Time and Money". AASHTO News Release, March 27, 2018 Obtained from: https://news.transportation.org/Pages/NewsReleaseDetail.aspx?NewsReleaseID=1504

[7] Wheeler, P., "Use of Small Unmanned Aerial Systems for Land Surveying". FHWS-HIF-20-034. Federal Highway Administration. December 2019, 2019.

[8] Rogers, P., "Use of Small Unmanned Aerial Systems for Construction Inspection". FHWA-HIF-19-096. October 2019, 2019.

[9] Cheyne, D., Merrill, B., and Boggs, J., "Use of Small Unmanned Aerial Systems for Bridge Inspection". FHWA-HIF-19-056 October 2019, 2019.

[10] AASHTO, "Manual for Bridge Evaluation, 3rd Edition". American Association of State Highway and Transportation Officials, Washington DC, 2018.

[11] Transportation, U.S.D.o., "Bridge Inspector's Reference Manual". Federal Highway Administration, Washington DC, 2012.

[12] Banks, E., Cook, S.J., Fredrick, G., et al., " NCHRP Scan 17-01: Successful Approaches for the Use of Unmanned Aerial Systems by Surface Transportation Agencies." Aurora and Associates, P.C., Lawrenceville, NC. Obtained from: http://onlinepubs.trb.org/onlinepubs/nchrp/docs/NCHRP20-68A_17-01.pdf, 2018.

[13] D. Lee, J. Kim, and D. Lee, "Robust concrete crack detection using deep learning-based semantic segmentation, "International Journal of Aeronautical and Space Sciences, vol. 20, no. 1, pp. 287–299, Mar 2019.

[14] S. Dorafshan, R. J. Thomas, and M. Maguire, "Comparison of deep convolutional neural networks and edge detectors for image-based crack detection in concrete, "Construction and Building Materials, vol. 186, pp. 1031 – 1045, 2018.

[15] T. Rakha, A. Liberty, A. Gorodetsky, B. Kakillioglu, and S. Velipasalar, "Heat mapping drones: An autonomous computer-vision-based procedure for building envelope inspection using unmanned aerial systems (UAS)," Technology—Architecture + Design, vol. 2, no. 1,pp. 30–44, 2018.

[16] N. Michael, S. Shen, K. Mohta, Y. Mulgaonkar, V. Kumar, K. Nagatani, Y. Okada, S. Kirib-ayashi, K. Otake, K. Yoshida, K. Ohno, E. Takeuchi, and S. Tadokoro, "Collaborative map-ping of an earthquake-damaged building via ground and aerial robots," Journal of Field Robotics, vol. 29, no. 5, pp. 832–841, 2012.

[17] G. Morgenthal and N. Hallermann, "Quality assessment of unmanned aerial vehicle (uav) based visual inspection of structures," Advances in Structural Engineering, vol. 17, no. 3,pp. 289–302, 2014.

[18] S. S. Congress, A. J. Puppala, and C. L. Lundberg, "Total system error analysis of UAV-crp technology for monitoring transportation infrastructure assets, "Engineering Geology, vol.247, pp. 104 – 116, 2018.

[19] S. Rathinam, Z. W. Kim, and R. Sengupta, "Vision-based monitoring of locally linear structures using an unmanned aerial vehicle, "Journal of Infrastructure Systems, vol. 14,no. 1, pp. 52–63, 2008.

[20] E. Frew, T. McGee, ZuWhan Kim, Xiao Xiao, S. Jackson, M. Morimoto, S. Rathinam, J. Padial, and R. Sengupta, "Vision-based road-following using a small autonomous air-craft," in2004 IEEE Aerospace Conference Proceedings (IEEE Cat. No.04TH8720), vol. 5, March 2004, pp. 3006–3015 Vol.5.

[21] B. Coifman, M. McCord, R. G. Mishalani, and K. Redmill, "Surface transportation surveil-lance from unmanned aerial vehicles," in Proc. of the 83rd Annual Meeting of the Transportation Research Board, 2004.

[22] A. Puri, K. Valavanis, and M. Kontitsis, "Generating traffic statistical profiles using un-manned helicopter-based video data," in Proceedings 2007 IEEE International Conference on Robotics and Automation, April 2007, pp. 870–876.

[23] J. Irizarry, M. Gheisari, and B. N. Walker, "Usability assessment of drone technology as safety inspection tools," Journal of Information Technology in Construction (ITcon),vol. 17, no. 12, pp. 194–212, 2012.

[24] M. Gheisari and B. Esmaeili, "Applications and requirements of unmanned aerial systems(uas) for construction safety, "Safety Science, vol. 118, pp. 230 – 240, 2019.

[25] D. Roca, S. Lag ̈uela, L. D ́ıaz-Vilari ̃no, J. Armesto, and P. Arias, "Low-cost aerial unit for outdoor inspection of building facades, "Automation in Construction, vol. 36, pp. 128 –135, 2013.

[26] S. Siebert and J. Teizer, "Mobile 3d mapping for surveying earthwork projects using an unmanned aerial vehicle (uav) system, "Automation in Construction, vol. 41, pp. 1 – 14,2014.

[27] B. Hubbard, H. Wang, M. Leasure, T. Ropp, T. Lofton, S. Hubbard, and S. Lin, "Feasibility study of uav use for rfid material tracking on construction sites," inProc., ASCE Annual International Conference, 2015, pp. 669–676.

[28] M.-C. Wen and S.-C. Kang, "Augmented reality and unmanned aerial vehicle assist in construction management," in Computing in Civil and Building Engineering (2014), 2014, pp. 1570–1577.

[29] J. J. Lin, K. K. Han, and M. Golparvar-Fard, A Framework for Model-Driven Acquisition and

Analytics of Visual Data Using UAVs for Automated Construction Progress Monitoring. American Society of Civil Engineers, 2015, pp. 156–164.

[30] A. Ellenberg, A. Kontsos, F. Moon, and I. Bartoli, "Bridge related damage quantification using unmanned aerial vehicle imagery, "Structural Control and Health Monitoring, vol. 23, no. 9, pp. 1168–1179, 2016.

[31] N. Metni and T. Hamel, "A uav for bridge inspection: Visual servoing control law with orientation limits, "Automation in construction, vol. 17, no. 1, pp. 3–10, 2007.

[32] L. Duque, J. Seo, and J. Wacker, "Bridge deterioration quantification protocol using uav," Journal of Bridge Engineering, vol. 23, no. 10, 2018,

[33] J. Seo, L. Duque, and J. Wacker, "Drone-enabled bridge inspection methodology and application," Automation in Construction, vol. 94, pp. 112 – 126, 2018.

[34] A. E. Jimenez-Cano, P. J. Sanchez-Cuevas, P. Grau, A. Ollero, and G. Heredia, "Contact-based bridge inspection multirotor: Design, modeling, and control considering the ceiling effect," IEEE Robotics and Automation Letters, vol. 4, no. 4, pp. 3561–3568, Oct 2019.

[35] P. J. Sanchez-Cuevas, P. Ramon-Soria, B. Arrue, A. Ollero, and G. Heredia, "Robotic system for inspection by contact of bridge beams using UAVs," Sensors, vol. 19, no. 2, 2019.

[36] "Final Report (MN/RC 2015-40)," Unmanned Aerial Vehicle Bridge Inspection Demonstration Project, 2015, Minnesota Department of Transportation (MnDOT).

[37] A. Ishizaka and S. Siraj, "Are multi-criteria decision-making tools useful? an experimental comparative study of three methods, "European Journal of Operational Research, vol. 264, no. 2, pp. 462 – 471, 2018.

[38] F. Craveiro, J. P. Duarte, H. Bartolo, and P. J. Bartolo, "Additive manufacturing as an enabling technology for digital construction: A perspective on construction 4.0," Automation in Construction, vol. 103, pp. 251 – 267, 2019.

[39] M. Pavan and R. Todeschini, "1.19 - multicriteria decision-making methods," incomprehensive Chemometrics, S. D. Brown, R. Tauler, and B. Walczak, Eds. Oxford: Elsevier,2009, pp. 591 – 629.

[40] J.-J. Wang, Y.-Y. Jing, C.-F. Zhang, and J.-H. Zhao, "Review on multi-criteria decision analysis aid in sustainable energy decision-making, "Renewable and Sustainable Energy Reviews, vol. 13, no. 9, pp. 2263 – 2278, 2009.

[41] W. Edwards, "How to use multi-attribute utility measurement for social decision making," IEEE Transactions on Systems, Man, and Cybernetics, vol. 7, no. 5, pp. 326–340, May1977.

[42] W. Edwards and D. von Winterfeldt, "Decision analysis and behavioral research, "Cambridge University Press, vol. 604, pp. 6–8, 1986.

[43] R. L. Keeney and H. Raiffa, "Decisions with multiple objectives: preferences and value trade-offs," Cambridge university press, 1993.

[44] R. Saaty, "The analytic hierarchy process what it is and how it is used," Mathematical Modelling, vol.

9, no. 3, pp. 161 – 176, 1987.

[45] S. Pohekar and M. Ramachandran, "Application of multi-criteria decision making to sustainable energy planning—a review, "Renewable and Sustainable Energy Reviews, vol. 8, no. 4, pp. 365 – 381, 2004.

[46] S. HekmatiAthar, D. Ziaei, and N. Goudarzi, "Artificial UAV 3ligence for optimal sitting of individual and networks of wind farms," in Proc. of the ASME Power Conference, July2019.

[47] D. Kalan and M. E. Ozbek, "Development of a construction project bidding decision-making tool, "Practice Periodical on Structural Design and Construction, vol. 25, no. 1, p.04019032, 2020.

[48] P. Ben ́ıtez, E. Rocha, H. Varum, and F. Rodrigues, "A dynamic multi-criteria decision-making model for the maintenance planning of reinforced concrete structures," Journal of Building Engineering, vol. 27, p. 100971, 2020.

[49] F. Pomponi, A. Moghayedi, L. Alshawawreh, B. D'Amico, and A. Windapo, "Sustainability of post-disaster and post-conflict sheltering in Africa: What matters?" Sustainable Production and Consumption, vol. 20, pp. 140 – 150, 2019.

[50] H. R. Francisco, A. Fabr ́ıcio Corrˆeia, and A. Feiden, "Classification of areas suitable for fish farming using geotechnology and multi-criteria analysis," ISPRS International Journal of Geo-Information, vol. 8, no. 9, 2019.

[51] E. K. Zavadskas, R. Bausys, and I. Mazonaviciute, "Safety evaluation methodology of urban public parks by multi-criteria decision making, "Landscape and Urban Planning, vol. 189, pp. 372 – 381, 2019.

[52] K. Liaw, "Simulation of flow around bluff bodies and bridge deck sections using cfd,"2005. [Online]. Available: http://eprints.nottingham.ac.uk/10125/

[53] W. Huang, Q. Yang, and H. Xiao, "Cfd modeling of scale effects on turbulence flow and scour around bridge piers, "Computers & Fluids, vol. 38, no. 5, pp. 1050 – 1058, 2009, advances in Computational Fluid Dynamics.

[54] S. Shirai and T. Ueda, "Aerodynamic simulation by cfd on flat box girder of super-long-span suspension bridge," Journal of Wind Engineering and Industrial Aerodynamics, vol. 91,no. 1, pp. 279 – 290, 2003, fifth Asia-Pacific Conference on Wind Engineering.

[55] I. A. Herrera, A. O. Nordskag, G. Myhre, and K. Halvorsen, "Aviation safety and maintenance under major organizational changes, investigating non-existing accidents, "Accident Analysis & Prevention, vol. 41, no. 6, pp. 1155 – 1163, 2009, accident Modelling and Prevention at ESREL 2006.

[56] D. Jones and M. Endsley, "Sources of situation awareness errors in aviation, "Aviation, space, and environmental medicine, vol. 67, pp. 507–12, 07 1996.

[57] M. Endsley, "Endsley, m.r.: Toward a theory of situation awareness in dynamic systems. Human factors journal 37(1), 32-64," Human Factors: The Journal of the Human Factors and Ergonomics Society, vol. 37, pp. 32–64, 03 1995.

[58] Federal Aviation Administration. "Recreational flyers & modeler communitybased organizations." [Online].Available: https://www.faa.gov/uas/recreationalfliers/18

[59] Zink, J.H., B., and Lovelace, B., "Unmanned Aerial Vehicles Enable Safe and Cost-Effective Bridge Inspection". Minnesota Department of Transportation Technical Summary 2015-40TS, 2015.

[60] Brooks, C., Dobson, R., Banach, D., et. al., "Evaluating the use of Unmanned Aerial Vehicles for Transportation Purposes". Michigan Tech Research Institute. Houghton, MI, 2015.

[61] Stacom, D., "DOT takes to the air to Inspect New London Bridge". Hartford Courant., 2016.

[62] Wells, J., and Lovelace, B., "Unmanned Aircraft System Bridge Inspection Demonstration Project Phase II Final Report". Report No. MN/RC 2017-18. Minnesota Department of Transportation, St. Paul, MN., 2017.

[63] Gillins, D.T., Parrish, C., Gillins, M.N., and Simpson, C., "Eyes in the Sky: Bridge Inspections with Unmanned Aerial Vehicles". Final Report SPR 787. Oregon Department of Transportation, Salem, OR, and Federal Highway Administration, Washington DC, 2018.

[64] Gillins, M., "Unmanned Aircraft Systems for Bridge Inspection: Testing and Developing End-to-End Operational Workflow". Master's Thesis. Oregon State University, Corvallis, OR., 2016.

[65] "Morrisville, NC Weather Underground | Weather History", TWC Product and Technology, https://www.wunderground.com/history/daily/us/nc/morrisville/KRDU. Accessed 7/16/2021

[66] Deters, R.W., Krishnan, G.K.A, and Selid, M.S., "Reynold Number Effects on the Performance of Small-Scale Propellers". In Proceedings of the 32nd AIAA Applied Aerodynamics Conference, Atlanta, GA, USA, 16-20 June 2014, pp. 1-43, 2014.

[67] Brandt, J.B., and Selig, M.S, "Propeller Performance Data at Low Reynolds Numbers". In the Proceedings of the 49th AIAA Aerospace Sciences Meeting, Grapevine, TX, USA, 7-10 January 2013, pp. 1-18, 2013.

[68] G. Shuxia, D. Zhongyao, H. Zhantao, and H. Chufeng, "Simulation of dynamic electromagnetic interference environment for unmanned aerial vehicle data link," China Communications, vol. 10, no. 7, pp. 19–28, 2013.

[69] A. Hailemichael, M. Behniapoor, and A. Karimoddini, "Development of an interval type-2 tsk fuzzy logic attitude controller for UAV," in2018 International Conference on Unmanned Aircraft Systems (ICUAS), 2018, pp. 1003–1009.

[70] M. Behniapoor, Zhuoning Yuan, A. Hailemichael, K. V. B. Bowles, A. Karimoddini, and A. Homaifar, "Development of a micro aerial vehicle," in2016 World Automation Congress (WAC), 2016, pp. 1–6.

[71] F. Box, L. Globus, Y.-S. Hoh, R. Snow, and J. Chadwick, "Potential rf interference to control links of small, unmanned aircraft," in 2008 Integrated Communications, Navigation and Surveillance Conference, 2008, pp. 1–12.

[72] J. Natarian, "Effects of radio frequency interference on an 802.11a wireless ad-hoc network," in Proceedings of the IEEE 2010 National Aerospace Electronics Conference, 2010, pp.237–239.

[73] W. Huang, L. D. Otero, C. Otero, and M. Moyou, "Impact of camera vibration frequencies on image

noise for unmanned aerial system applications," Southeast Con 2018, pp. 1–5, 2018.

[74] M. Verma, V. Lafarga, M. Baron, and C. Collette, "Active stabilization of unmanned aerial vehicle imaging platform," Journal of Vibration and Control, vol. 26, no. 19-20, pp.1791–1803, 2020. [Online]. Available: https://doi.org/10.1177/1077546320905494

[75] J. Afman, L. Ciarletta, E. Feron, J. Franklin, T. Gurriet, and E. N. Johnson, "Towardsa new paradigm of UAV safety,"CoRR, vol. abs/1803.09026, 2018. [Online]. Available: http://arxiv.org/abs/1803.09026

[76] M. Maguire and P. Szary, "Unmanned aerial vehicle augmented bridge inspection feasibility study," inIdaho Transportation Department Report, 2016.

[77] J. Verbeke, "Experimental maneuverability and agility quantification for rotary unmanned aerial vehicle," International Journal of Micro Air Vehicles, vol. 10, 10 2017.

[78] Harcon, Bridge rigging. [Online]. Available: https://www.harconcorp.com/wp-content/uploads/2018/06/rigging-09.jpg

[79] MEC and F Expert Engineers. [Online]. Available: https://4.bp.blogspot.com/-uxBAXrvq7E/V8V02WGgXvI/AAAAAAAA7ME/3AD6bMmckFgwz4YLXQtTkK2bFA-GoZl3wCLcB/s1600/bridgeriggers4.jpg

[80] Toronto Star, On assignment: hanging from the bloor viaduct bridge. [Online]. Available: https://projects.thestar.com/photos/onassignment/2015/02/02/stars-behind-the-scenes-rope-access-maintenance.html

[81] T. Zhao, D. Doll, D. Wang, and Y. Chen, "A new framework for uav-based remote sensing data processing and its application in almond water stress quantification," 2017 International Conference on Unmanned Aircraft Systems (ICUAS), 2017, pp. 1794–1799.

[82] S. Waharte and N. Trigoni, "Supporting search and rescue operations with uavs," in 2010 International Conference on Emerging Security Technologies, 2010, pp. 142–147.

[83] A. Girma, N. Bahadori, M. Sarkar, T. G. Tadewos, M. R. Behnia, M. N. Mahmoud, A. Karimoddini, and A. Homaifar, "Iot-enabled autonomous system collaboration for disaster-area management," IEEE/CAA Journal of Automatica Sinica, vol. 7, no. 5, pp.1249–1262, 2020.

[84] M. A. Balaban, T. W. Mastaglio, and C. J. Lynch, "Analysis of future uas-based delivery," in2016 Winter Simulation Conference (WSC), 2016, pp. 1595–1606.

[85] Z. Zaheer, A. Usmani, E. Khan, and M. A. Qadeer, "Aerial surveillance system using uav," in 2016 Thirteenth International Conference on Wireless and Optical Communications Networks (WOCN), 2016, pp. 1–7.

[86] N. Namvar, A. Homaifar, A. Karimoddini, and B. Maham, "Heterogeneous uav cells: An Effective resource allocation scheme for maximum coverage performance," IEEE Access, vol. 7, pp. 164 708–164 719, 2019.

[87] K. Vinh, S. Gebreyohannes, and A. Karimoddini, "An area-decomposition based approach for cooperative tasking and coordination of UAVs in a search and coverage mission," in 2019 IEEE Aerospace Conference, 2019, pp. 1–8.

[88] S. HekmatiaAdhar, N. Goudarzi, A. Karimoddini, A. Homaifar, and D. Divakaran, "Asystematic evaluation and selection of UAS-enabled solutions for bridge inspection practices," in 2020 IEEE Aerospace Conference, 2020, pp. 1–11.

[89] J. Zink and L. Barritt, "Evaluating the use of unmanned aerial vehicles for transportation purposes," in Final Report, 2015.

[90] S. Dorafshan and M. Maguire, "Bridge inspection: human performance, unmanned aerial systems and automation," Journal of Civil Structural Health Monitoring, vol. 8, 07 2018.

[91] S. Abu Dabous, S. Yaghi, S. Alkass, and O. Moselhi, "Concrete bridge deck condition assessment using IR thermography and ground penetrating radar technologies," Automation in Construction, vol. 81, pp. 340–354,2017. [Online]. Available: https://www.sciencedirect.com/science/article/pii/S0926580517303229

[92] E. Mahama, T. Walpita, A. Karimoddini, A. Eroglu, N. Goudarzi, T. Cavalline, and M. Khan, "Testing and evaluation of radio frequency immunity of unmanned aerial vehicles for bridge inspection," in 2021 IEEE Aerospace Conference (50100), 2021, pp. 1–8.

[93] F. Giacobbe and E. Biancuzzo, "Inspection of components with the support of the drones," International Research Journal of Engineering and Technology (IRJET), vol. 5, p. 1784, 122018.

[94] J. X. J. Bannwarth, Z. J. Chen, K. A. Stol, B. A. MacDonald, and P. J. Richards, "Development of a wind tunnel experimental setup for testing multirotor unmanned aerial vehicles in turbulent conditions," in 2018 IEEE/ASME International Conference on Advanced UAV 3ligent Mechatronics (AIM), 2018, pp. 724–729.